



A11104 022428

OFFICIAL USE ONLY

NBS
PUBLICATIONS

NBSIR 78-1510

Intruder Detection Using Trace Constituent Analysis

J. R. DeVoe
D. M. Sweger
R. A. Velapoldi

Center for Analytical Chemistry
National Bureau of Standards

Prepared by
Law Enforcement Standards Laboratory
Center for Consumer Product Technology
National Bureau of Standards
Washington, D.C. 20234

May 1979

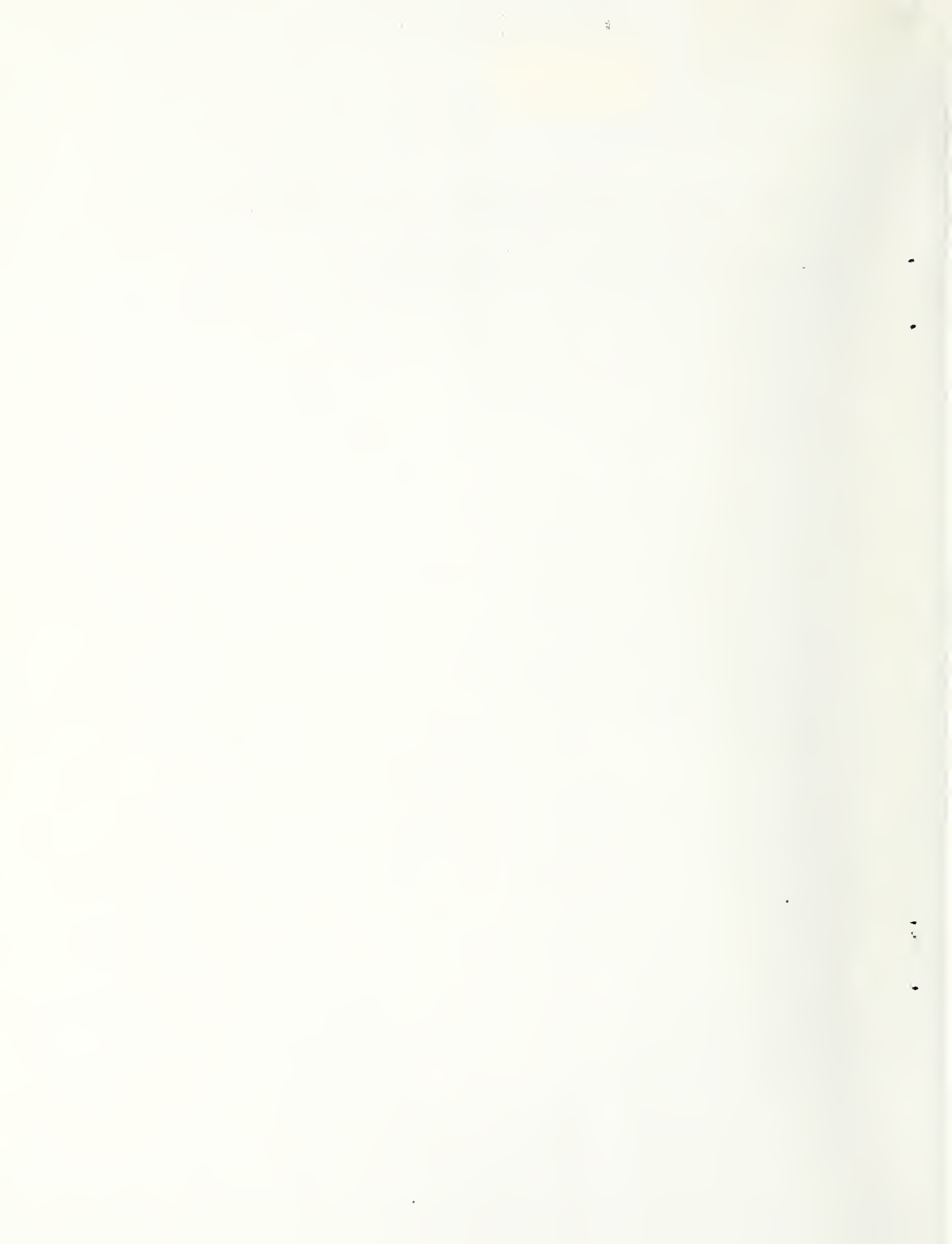
Progress Report

Prepared for
Nuclear Surety Directorate
Defense Nuclear Agency
Washington, D.C. 20305

QC
100
U56
78-1510
C.2

Work was sponsored by the Defense Nuclear Agency under
Work Code PQ99QAX DE910 and Work Unit Code 31

OFFICIAL USE ONLY



National Bureau of Standards
SEP 25 1979
NOT ACC-CLER
QC100
456
N2-1510
C. 2

OFFICIAL USE ONLY

NBSIR 78-1510

INTRUDER DETECTION USING TRACE CONSTITUENT ANALYSIS

J. R. DeVoe
D. M. Sweger
R. A. Velapoldi

Center for Analytical Chemistry
National Bureau of Standards

Prepared by
Law Enforcement Standards Laboratory
Center for Consumer Product Technology
National Bureau of Standards
Washington, D.C. 20234

May 1979

Progress Report

Prepared for
Nuclear Surety Directorate
Defense Nuclear Agency
Washington, D.C. 20305

This work was sponsored by the Defense Nuclear Agency under
Subtask Code PQ99QAX DE910 and Work Unit Code 31



U.S. DEPARTMENT OF COMMERCE, Juanita M. Kreps, Secretary

Jordan J. Baruch, Assistant Secretary for Science and Technology

U.S.
NATIONAL BUREAU OF STANDARDS, Ernest Ambler, Director

OFFICIAL USE ONLY

ACKNOWLEDGMENTS

This document was prepared by the Law Enforcement Standards Laboratory of the National Bureau of Standards under the direction of Lawrence K. Eliason, Manager, Security Systems Program, and Jacob J. Diamond, Chief of LESL.

OFFICIAL USE ONLY

Foreword

The Defense Nuclear Agency (DNA) is engaged in a continuing effort to enhance the security of nuclear weapons storage. In this effort, it is receiving technical support from the National Bureau of Standards' Law Enforcement Standards Laboratory (LESL), whose overall program involves the application of science and technology to the problems of crime prevention, law enforcement and criminal justice.

LESL is supporting DNA's physical security program in the behavioral science, the chemical science and the ballistic materials areas, among others.

Among the tasks being performed by LESL for DNA are the preparation and publication of several series of technical reports on the results of its researches. This document is one such report.

Technical comments and suggestions are invited from all interested parties. They may be addressed to the authors or to the Law Enforcement Standards Laboratory, National Bureau of Standards, Washington, D.C. 20234.

Jacob J. Diamond
Chief, Law Enforcement Standards
Laboratory

OFFICIAL USE ONLY

Contents

	Page
I. Introduction	1
II. Particle Luminescence	2
Phase 1. Characterization of Candidate Particles	3
Phase 2. Types of Uniquely Tagged Particles . .	22
Phase 3. Methods of Deployment	22
Phase 4. Evaluation of the Sensitivity	23
Countermeasures	24
III. Infrared Lasers for Trace Gas Analysis	25
Phase 1. Establish Limits of Detection and Feasibility for Isotopic Ratio Measurements	27
Formaldehyde	30
Laser Ranging Chemical Analysis	30
IV. The Olfactory Receptor as an Analytical Instrument	36
References	41
Appendix A--Assignment of Vibration-Rotation Energy Levels in Formaldehyde	43



OFFICIAL USE ONLY

I. INTRODUCTION

This research project is based on the following scenario for an intruder deterrent and detection system. The basic assumption is that an intruder has entered a secured space and has thereby set off an alarm that alerts guards and triggers mechanisms which release and disperse one or more chemical substances. The functions of the chemicals are to: (1) Act as an immediate deterrent by producing low visibility and/or a noxious atmosphere causing choking, nausea, etc., and (2) to adhere to the intruder so that he can be traced and unequivocally identified if he escapes.

The intruder detection system envisions the use of two distinct chemical analyzers. The first is an on-site chemical gas analyzer that has moderate sensitivity and quick response (e.g., seconds), and is either portable or able to quickly scan a large area. This chemical analyzer should provide clues to the direction of the intruder's flight.

The second is an off-site chemical analyzer that can be used to detect the chemical on the intruder's person or in space that he has occupied. This analyzer should have the highest possible sensitivity and should be able to identify the taggant chemical uniquely, with few or no false positives. It

OFFICIAL USE ONLY

would be desirable if this instrument were portable or at least semi-portable (e.g., in a small truck or van).

The remainder of this report discusses three chemical analysis techniques that should be suitable [8].*

II. PARTICLE LUMINESCENCE

Particles containing a luminescent material can be incorporated into a spray system which, when triggered by an intruder, would disperse the particles throughout a room. If the intruder manages to escape from the secured space, a trail of particles should be observable with appropriate detection equipment. This technique is similar to that recently demonstrated for the tagging of explosives [1]. The particles can be fabricated in such a way that unique identification is possible. This is accomplished by adding known mixtures of luminescent substances to various glass formulations and then converting them to glass microspheres. The luminescent spectra of these particles, coupled with their sphericity, uniquely identify them.

The purpose of this project is to explore the possibility of fabricating such particles and to suggest possible methods for their use. There are five phases to this project.

1. Characterization of candidate particles.
2. Exploration of the extent of unique types of tagged particles.

*Numbers in brackets refer to the references on page 41.

OFFICIAL USE ONLY

3. Experimentation with various methods of deployment.
4. Evaluation of the sensitivity of the tagging system.
5. Evaluation of the effectiveness of the system by means of field tests.

Phase 1. Characterization of Candidate Particles

The luminiscence spectra of the glass microspheres were measured with the microspectrofluorimeter depicted in figure 1. Excitation radiation, produced by a xenon or mercury arc source, passes through a BG 38 red-suppression filter (transmitting radiation from 325 to 700 nm), and through a Ploem illuminator (dichroic mirror-barrier filter combination) to the sample. Three Ploem combinations were used: 1-1, which provided excitation over the range 325-400 nm ($\lambda_{\max} \approx 350$ nm); 2-2, which provides excitation from 350-450 nm ($\lambda_{\max} \approx 400$ nm); and 3-3, which provided excitation from 375 to 500 nm ($\lambda_{\max} \approx 450$ nm). In general the 1-1 or 2-2 combinations were used for sample excitation, since the barrier filter in the 3-3 combination distorts the emission spectrum below a wavelength of about 580 nm. The radiation emitted by the luminophor in the particle proceeds back through the dichroic mirror, the barrier filter, a measuring aperture and a 0.1 m grating monochromator, and is measured by a photomultiplier tube (S-20 response). The signal is amplified and the spectrum is recorded directly on an X-Y recorder.

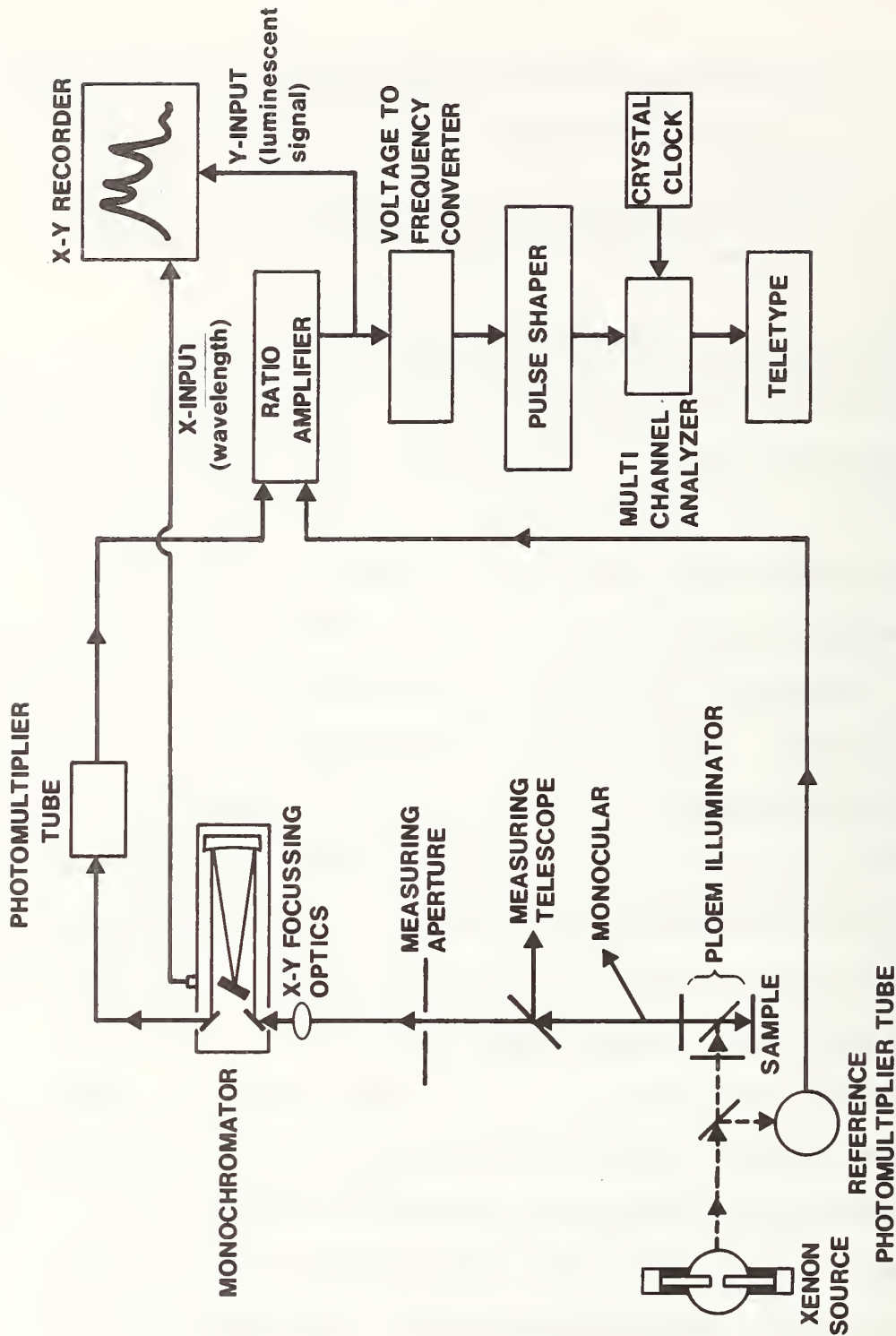


Figure 1. Block diagram of apparatus used for the determination of the luminance emission spectrum.

OFFICIAL USE ONLY

The microparticles used were glass beads containing a mixture of two rare earth and/or transition metal ion luminophors. The two ions selected for a particular melt had emission spectra in the green and the orange or red portions of the visible spectrum, respectively. The green luminophors included the terbium, copper, dysprosium, and uranyl ions while the orange and red luminophors were the samarium and europium ions, respectively [2]. The emission spectrum of each luminophor and the ratios of selected emission peaks of the two luminophors made it possible to identify uniquely the particle and its composition.

Several preliminary glass melts were made [3], with the compositions shown in the first seven columns of table 1; each of these contained two luminophores. Four additional glasses were made, each of which contained a single luminophore. Small portions of each of these melts were crushed and their spectra measured with the microspectrofluorimeter.

The spectra of the individual uranyl, europium, terbium, and samarium ions in glass are given in figures 2 and 3. The spectra of combinations of these and other inorganic ions are given in figures 4-12 and the instrumental conditions under which the spectra were recorded are summarized in table 2. Of the seven preliminary melts with two luminophores only sample

Table 1. Compositions of the preliminary glass melts.

Sample #	Composition, mole percent										YYY	XXX	YYY	
	1031	1032	1045	1064	1077	1078	1079	1079	1078	1077				
SiO ₂	56.0	56.0	56.0	56.0	56.0	56.0	56.0	56.0	56.0	56.0	56.0	56.0	56.0	56.0
ZnO	16.0	16.0	16.0	16.0	16.0	16.0	16.0	16.0	16.0	16.0	16.0	16.0	16.0	16.0
BaO	25.5	26.0	26.4	26.2	25.5	24.5	25.9	25.9	24.5	25.5	26.4	25.9	25.0	26.4
Eu ₂ O ₃	1.5	-	1.5	1.5	1.5	1.5	1.0	1.0	1.5	1.5	1.0	1.0	-	-
Sm ₂ O ₃	-	1.0	-	-	1.0	-	1.0	1.0	-	-	1.0	1.0	1.0	1.0
Tb ₂ O ₃	1.0	1.0	-	-	-	-	-	-	-	-	-	-	-	-
DY ₂ O ₃	-	-	-	-	-	2.0	-	-	2.0	-	-	-	2.0	-
U ₃ O ₈	-	-	-	0.3	-	-	-	-	-	-	-	-	-	0.6
CuO	-	-	0.1	-	-	-	-	0.1	-	-	-	0.1	-	-

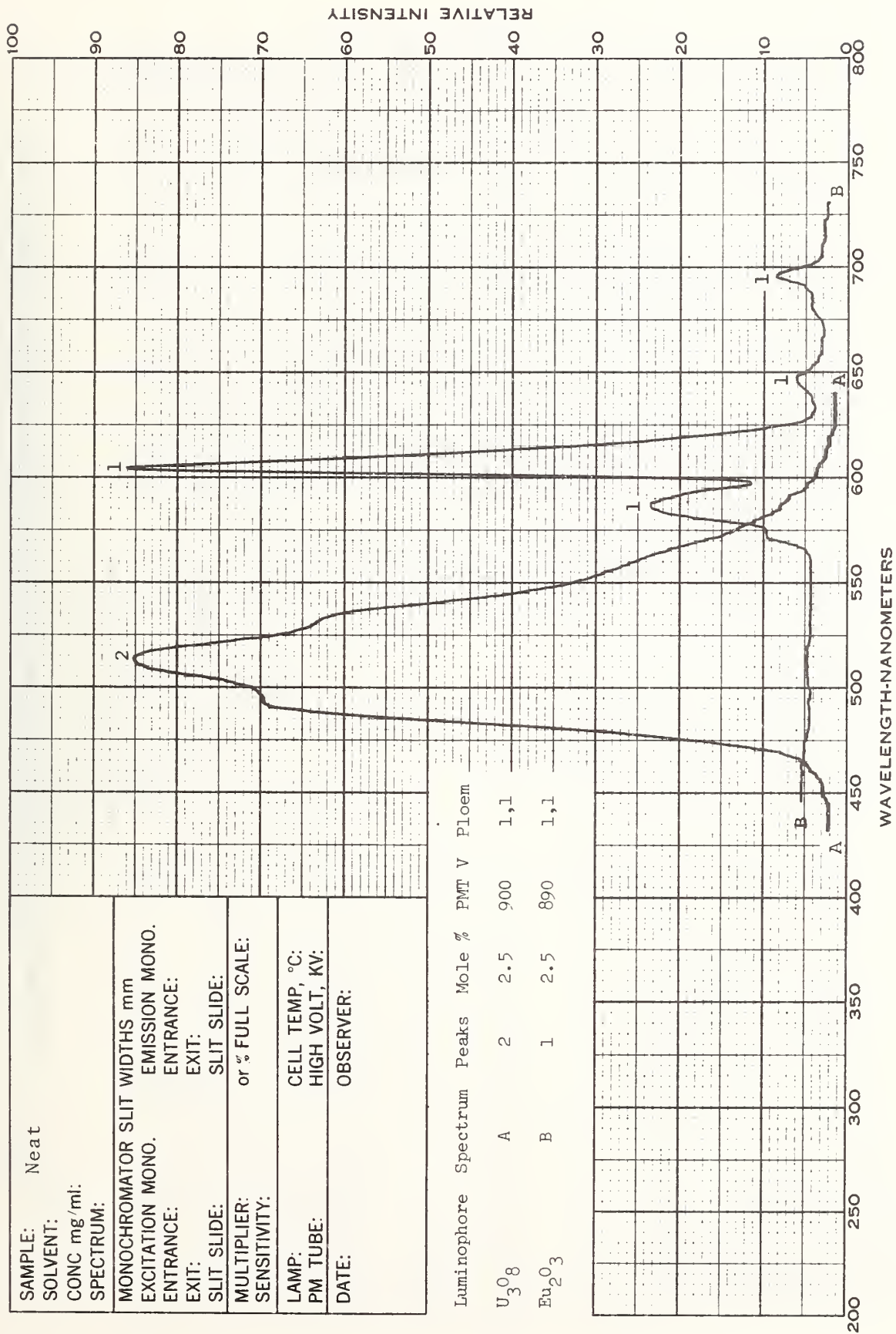


Figure 2. Luminescence spectra of glasses containing U₃O₈ and Eu₂O₃, respectively.

SAMPLE: Neat
 SOLVENT:
 CONC mg/ml:
 SPECTRUM:
 MONOCHROMATOR SLIT WIDTHS mm
 EXCITATION MONO. EMISSION MONO.
 ENTRANCE: ENTRANCE:
 EXIT: EXIT:
 SLIT SLIDE: SLIT SLIDE:
 MULTIPLIER: or % FULL SCALE:
 SENSITIVITY:
 LAMP: CELL TEMP, °C:
 PM TUBE: HIGH VOLT, KV:
 DATE: OBSERVER:

Lumino-phore	Spectrum	Peaks	Mole %	PMT V	Ploem
Tb ₂ O ₃	A	2	4.0	800	1,1
Sm ₂ O ₃	B	1	1.1	930	1,1

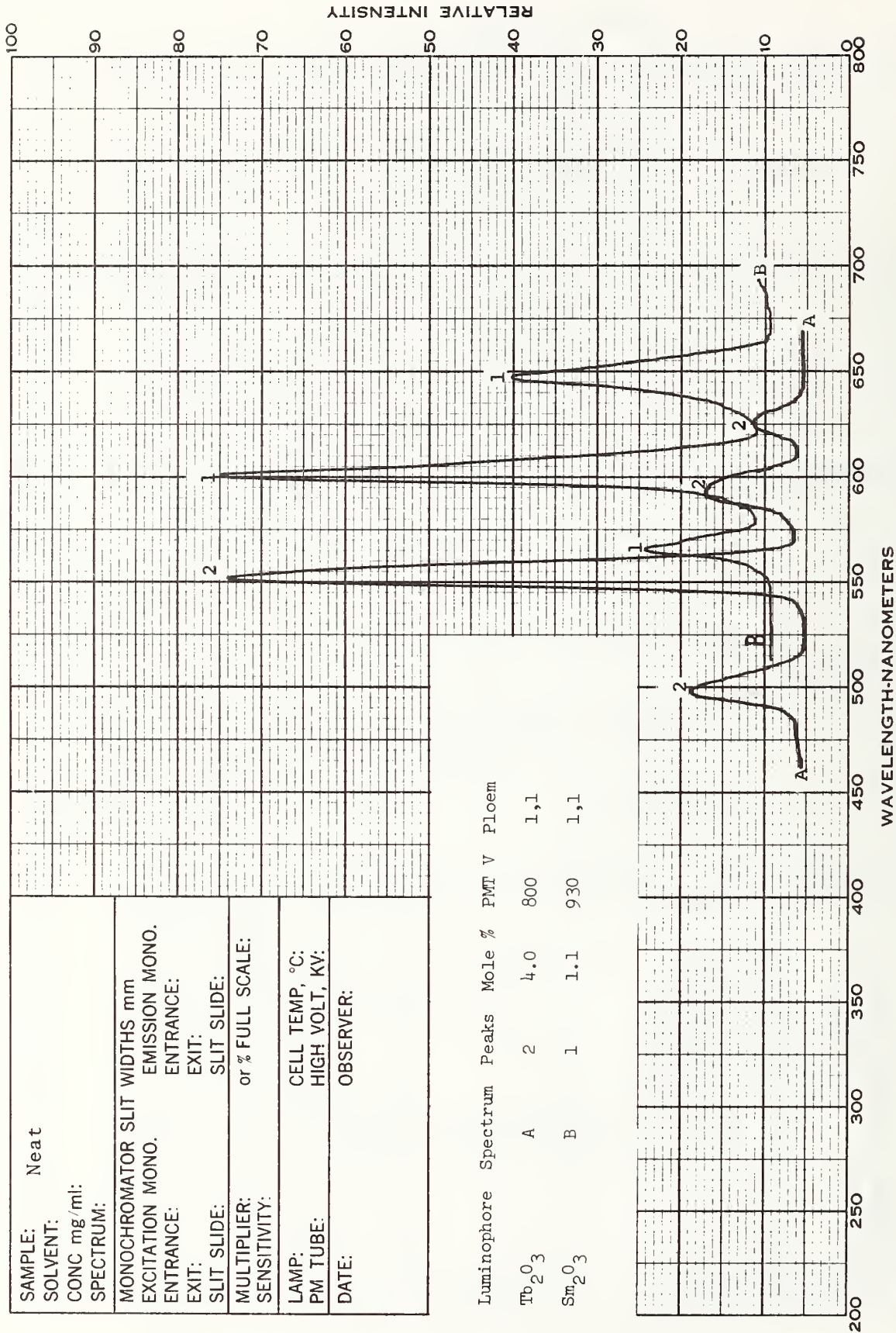


Figure 3. Luminescence spectra of glasses containing Tb₂O₃ and Sm₂O₃, respectively.

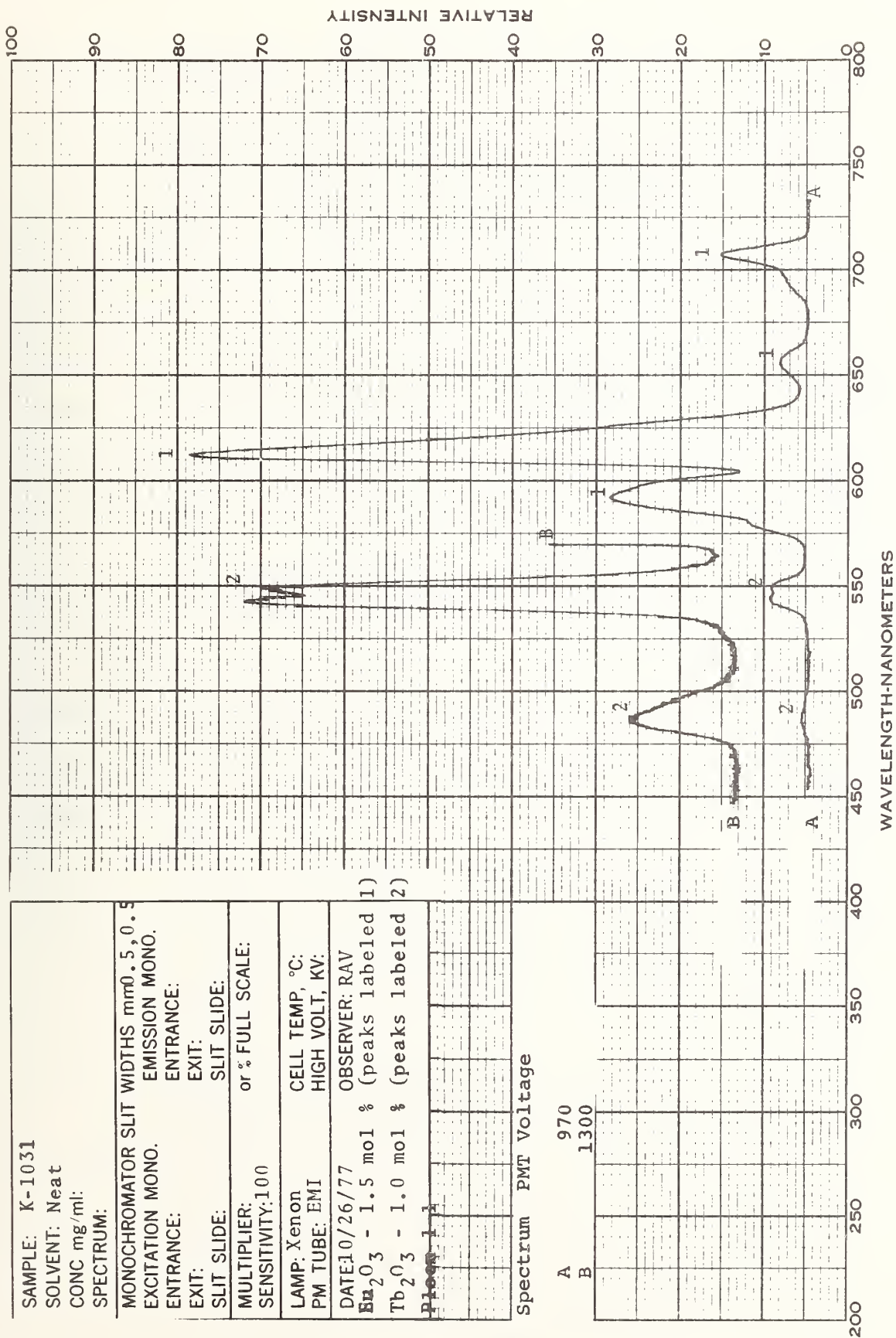


Figure 4. Luminescence spectra of a glass containing Eu₂O₃ and Tb₂O₃.

Table 2. Instrumental parameters for obtaining emission spectra of sample glass melts.

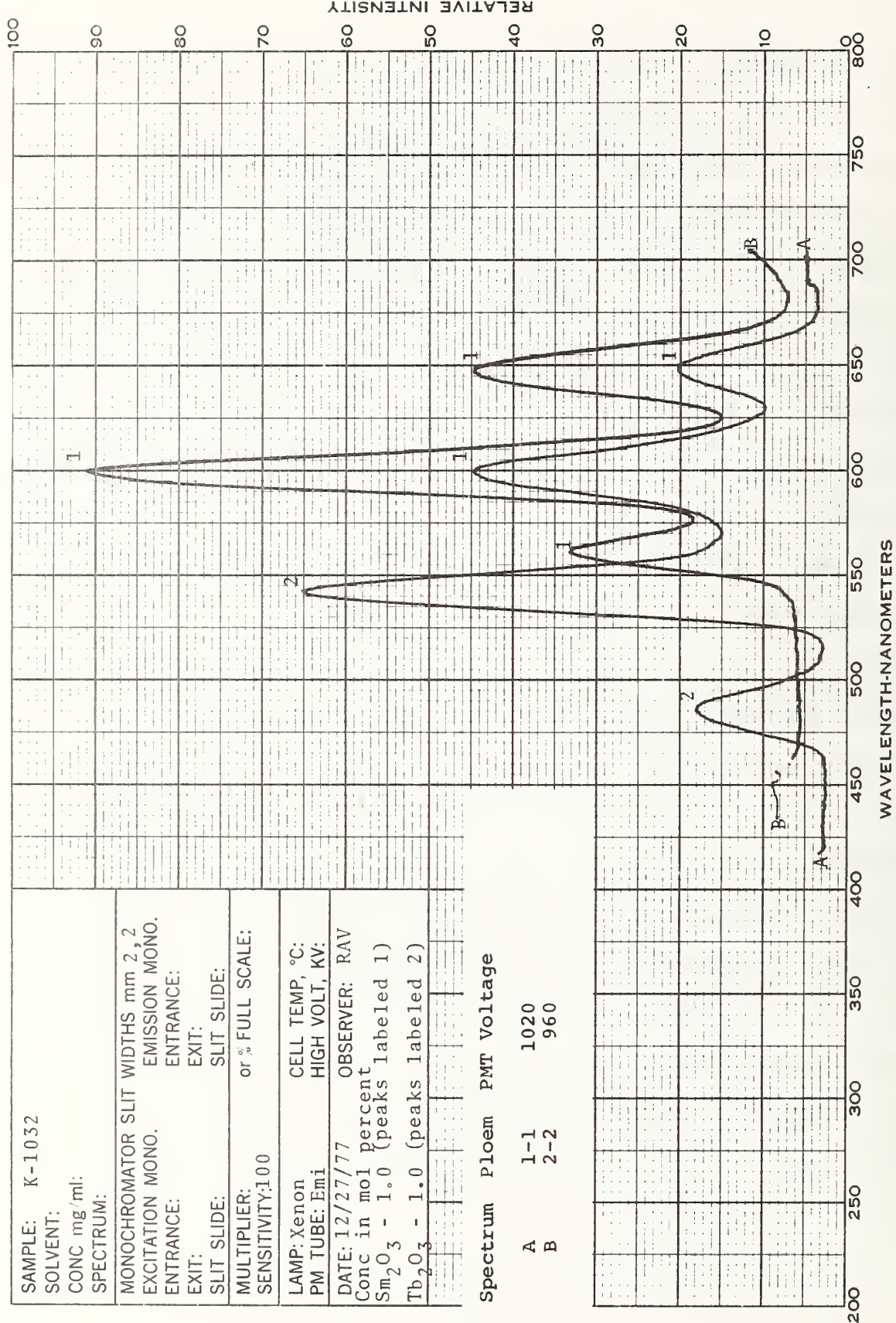
Figure	Sample #	Ions	Spectrum	Ploera	Slits (mm)	PMT (V)
2	-	UO ₂ ²⁺ , Eu ³⁺	A, B	1-1	-	900, 800
3	-	Tb ³⁺ , Sm ³⁺	A, B	1-1	-	800, 930
4	K-1031	Eu ³⁺ + Tb ³⁺	A, B	1-1	.5, .5	970, 1300
5	K-1032	Sm ³⁺ + Tb ³⁺	A, B	1-1, 2-2	2, 2	1020, 960
6	K-1032	Sm ³⁺ + Tb ³⁺	A, B	1-1, 2-2	.5, .5	1381, 1590
7	K-1032	Sm ³⁺ + Tb ³⁺	A, B	1-1	2, 2, .5, .5	900, 1170
8	K-1045	Eu ³⁺ + Cu ²⁺	A, B, C	1-1, 1-1, 2-2	2, 2	840, 1200, 830
9	K-1064	Eu ³⁺ + UO ₂ ²⁺	A, B, C	1-1, 2-2, 3-3	2, 2	180, 730, 607
10	K-1077	Zu ³⁺ + Sm ³⁺	A, B	1-1, 2-2	2, 2	767, 737
11	K-1078	Eu ³⁺ + Dy ³⁺	A, B, C	1-1, 1-1, 2-2	2, 2	1100, 1500, 1130
12	K-1079	Eu ³⁺ + Sm ³⁺ + Cu ²⁺	A, B	1-1, 2-2	2, 2	890, 890

OFFICIAL USE ONLY

K-1032, containing a mixture of Sm^{3+} and Tb^{3+} , gave emission peaks due to the individual ions that were of comparable intensities. The emission spectra of sample K-1032 using two Ploem combinations (1-1 and 2-2) for excitation and two monochromator slit widths (0.5 and 2.0 mm, corresponding to bandpasses of 4.25 and 17 nm, respectively), are shown in figures 5, 6 and 7. These figures show that using a 1-1 Ploem combination for excitation results in emission spectra in which the peaks attributable to both ions can be readily identified. On the other hand, use of the 2-2 Ploem excitation combination (figs. 5 and 6) results in emission spectra attributable only to the Sm^{3+} ion (i.e., selective excitation).

Although the use of 0.5 mm slits produces peaks with better spectral resolution, from which the identification of individual rare earth ion emission peaks can more easily be made (fig. 7), the sharpness of these peaks makes peak height measurement more difficult. The use of 2 mm slits, on the other hand, makes it easier to measure the peak heights and facilitates the determination of the relative ratios of the Tb^{3+} peak at ~ 544 nm and the Sm^{3+} peak at ~ 602 nm. The concomitant decrease in resolution does not hinder particle identification.

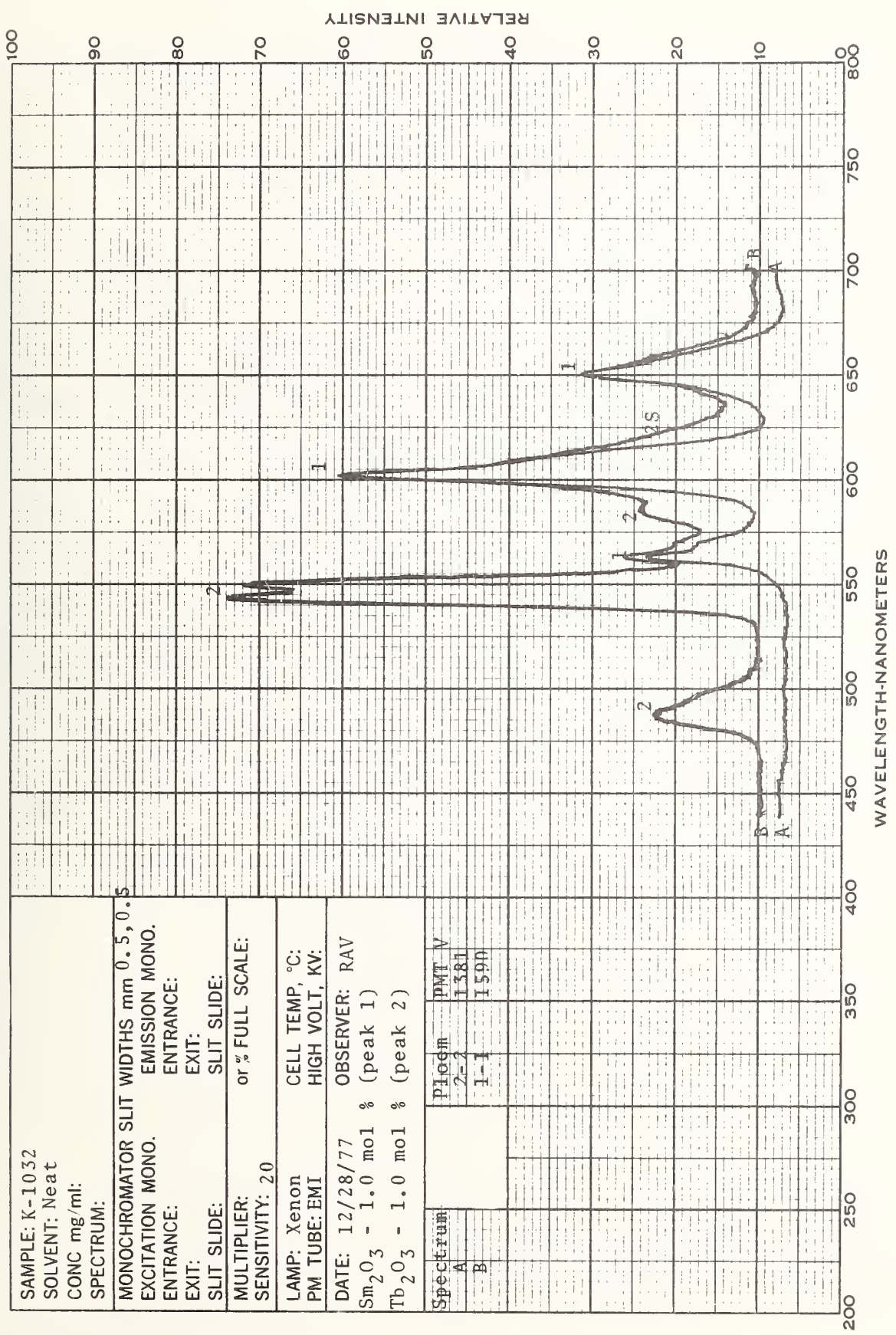
In all the other preliminary glass melts (samples K-1031, K-1045, K-1064, K-1077, K-1078 and K-1079), there appears to be



SAMPLE: K-1032
 SOLVENT:
 CONC mg/ml:
 SPECTRUM:
 MONOCHROMATOR SLIT WIDTHS mm 2, 2
 EMISSION MONO.
 ENTRANCE:
 EXIT:
 SLIT SLIDE:
 MULTIPLIER:
 SENSITIVITY:100
 LAMP: Xenon CELL TEMP, °C:
 PM TUBE: Emi HIGH VOLT, KV:
 DATE: 12/27/77 OBSERVER: RAV
 Conc in mol percent
 Sm₂O₃ - 1.0 (peaks labeled 1)
 Tb₂O₃ - 1.0 (peaks labeled 2)

Spectrum	Ploem	PMT Voltage
A	1-1	1020
B	2-2	960

Figure 5. Luminescence spectra of a glass containing Sm₂O₃ and Tb₂O₃.



SAMPLE: K-1032
 SOLVENT: Neat
 CONC mg/ml:
 SPECTRUM:
 MONOCHROMATOR SLIT WIDTHS mm 0.5, 0.5
 EXCITATION MONO. EMISSION MONO.
 ENTRANCE: ENTRANCE:
 EXIT: EXIT:
 SLIT SLIDE: SLIT SLIDE:
 MULTIPLIER: or % FULL SCALE:
 SENSITIVITY: 20
 LAMP: Xenon CELL TEMP, °C:
 PM TUBE: EMI HIGH VOLT, KV:
 DATE: 12/28/77 OBSERVER: RAV
 Sm₂O₃ - 1.0 mol % (peak 1)
 Tb₂O₃ - 1.0 mol % (peak 2)

Spectrum	pl	edm	PMT V
A	2-2	1-1	1581
B	1-1	1-1	1590

Figure 6. Same as figure 5 (different experimental conditions).

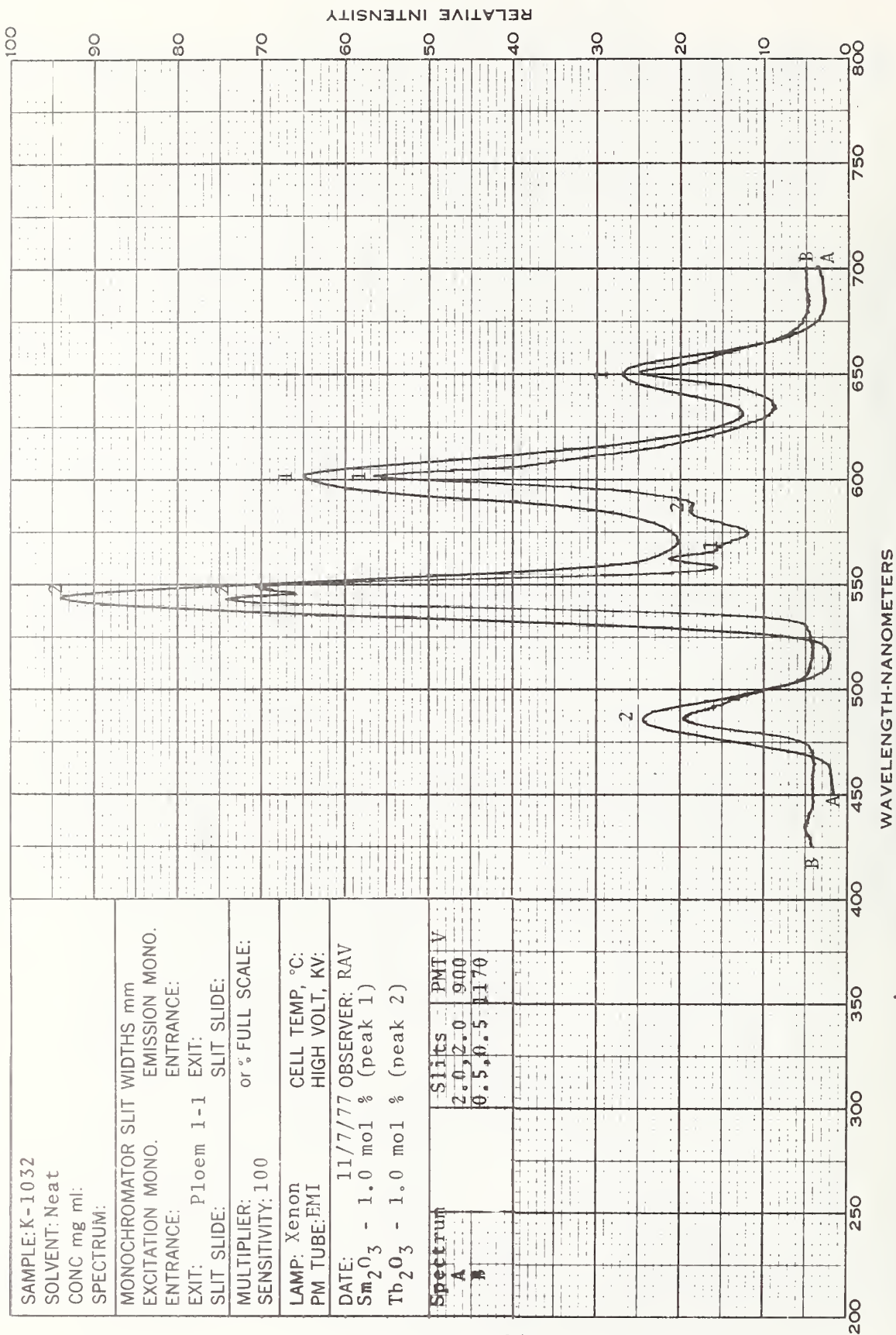


Figure 7. Same as figure 5 (different experimental conditions).

OFFICIAL USE ONLY

either luminescent quenching or extensive energy transfer from the green (Dy^{3+} , Cu^{2+} , Tb^{3+} , UO_2^{2+}) or orange (Sm^{3+}) emitting moiety to the red (Eu^{3+}) emitting moiety. In figure 4, the peaks due to Tb^{3+} emission can be identified at ~ 475 and 545 nm, but the intensities are much lower than would be expected if no quenching or energy transfer mechanisms were operating. Similarly, in figures 8-12, the samples exhibit emission spectra due mainly to the Eu^{3+} ion. In figure 8, a small peak at ~ 530 nm may be due to copper emission ($\lambda_{\text{max}} \approx 535\text{-}540$ nm in glasses); however, this peak is also visible in figure 11, which gives the emission spectra of a sample containing only Eu^{3+} and Dy^{3+} . Thus, this peak is probably due to very weak emissions from the second excited level of Eu^{3+} , i.e., $5D_1 \rightarrow F_{0,1,2}$ (1c).

A small peak at 545 nm in figure 9 is due to the UO_2^{2+} ion; however, its intensity is so low as to make it of no practical use. If any small peaks due to Sm^{3+} were present in figures 10 or 12, they would certainly be masked by the intense emissions due to Eu^{3+} . A small peak due to the emission from the Dy^{3+} species is present at 481 nm (fig. 11); however, it also is too low to be useful. The Dy^{3+} peak at 575 nm is completely masked by the Eu^{3+} emission.

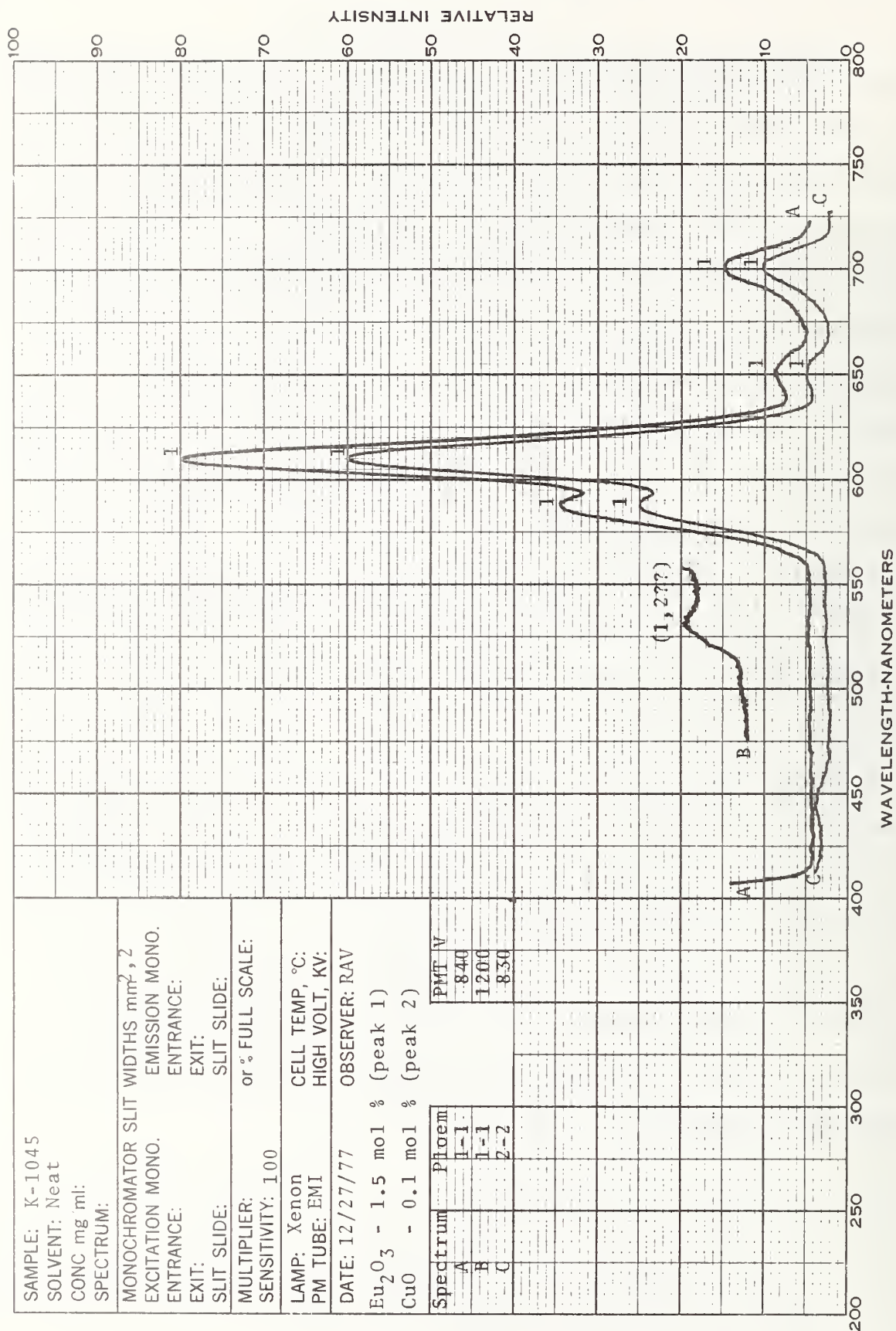


Figure 8. Luminescence spectra of a glass containing Eu₂O₃ and CuO.

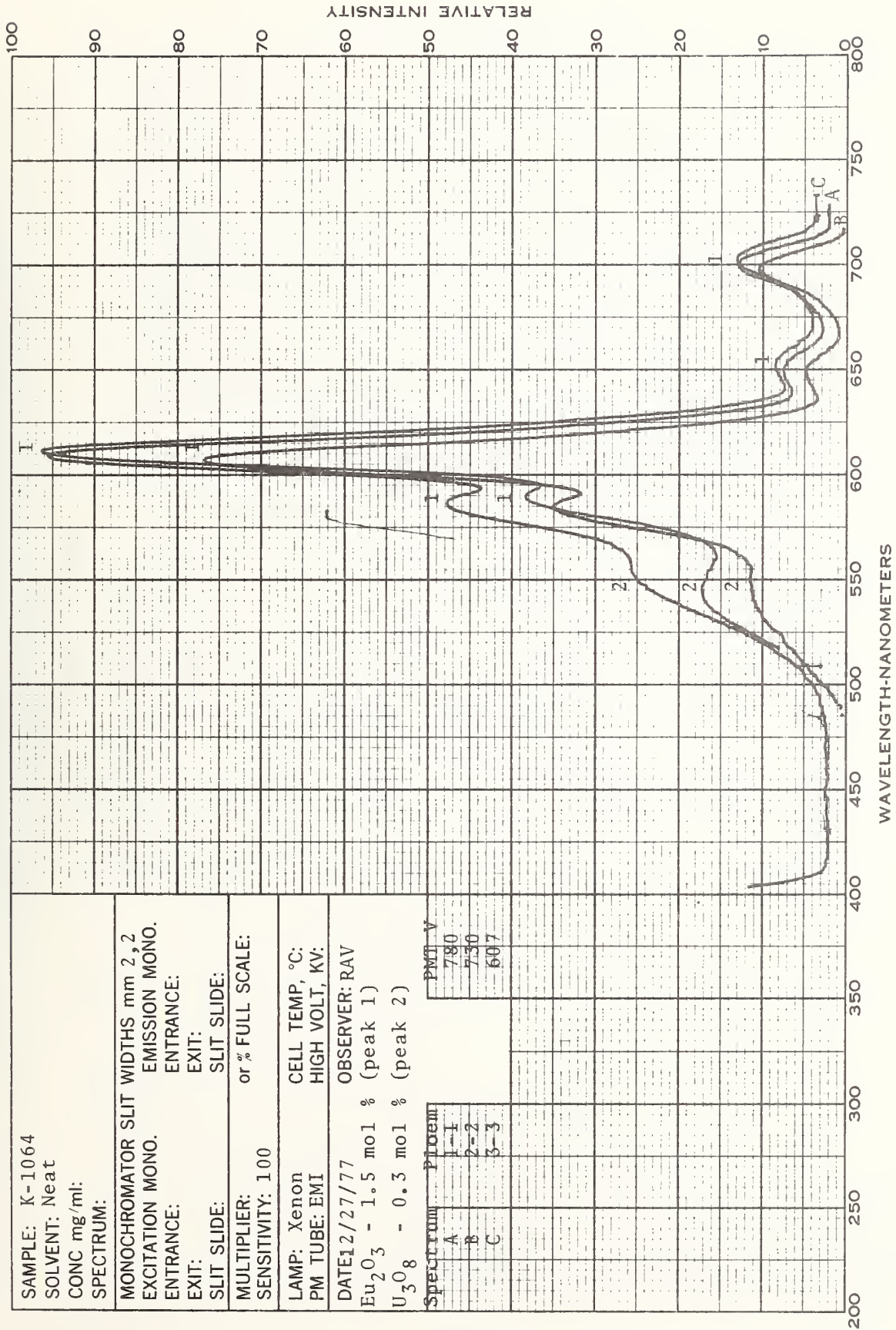


Figure 9. Luminescence spectra of a glass containing Eu₂O₃ and U₃O₈.

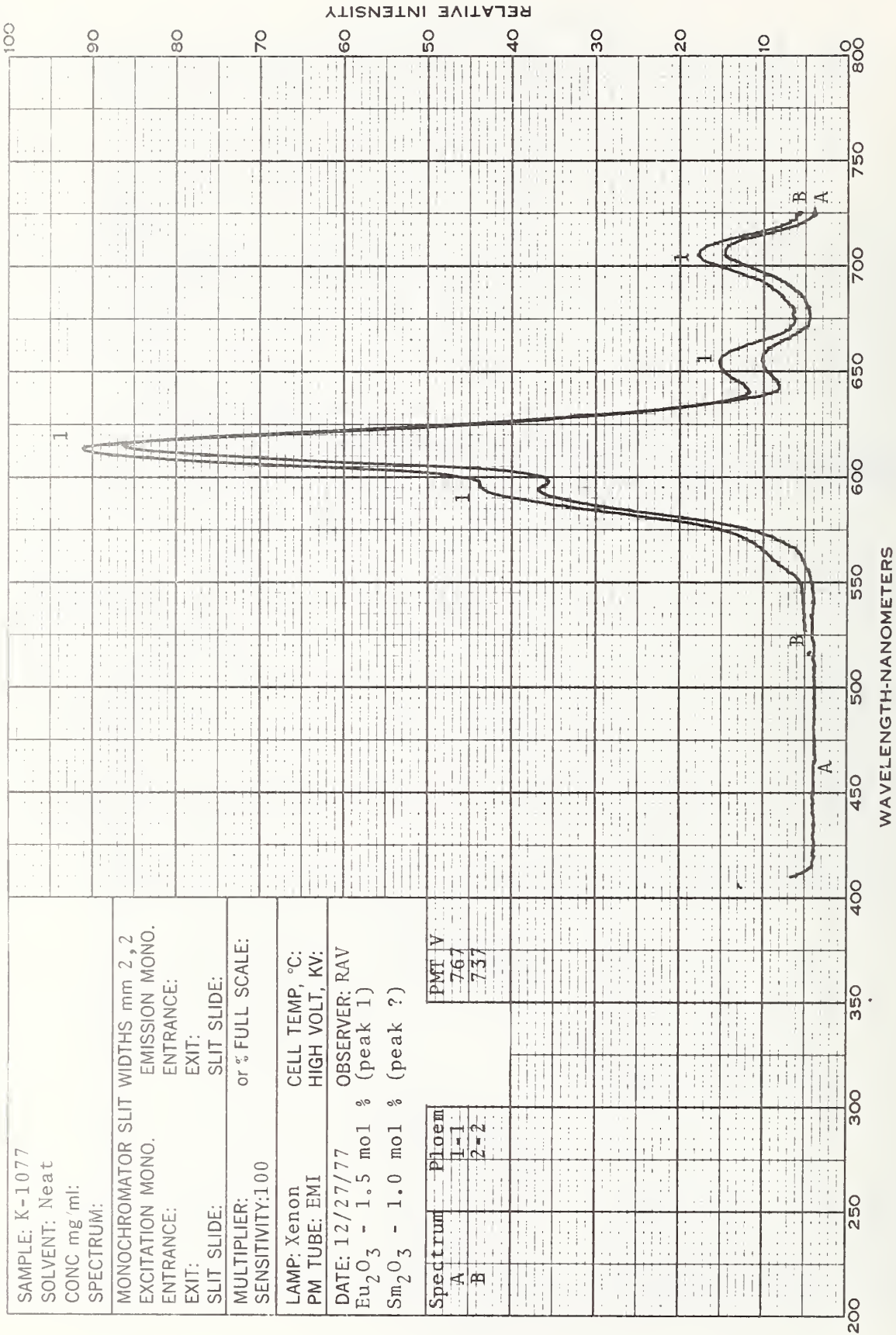


Figure 10. Luminescence spectra of a glass containing Eu_2O_3 and Sm_2O_3 .

SAMPLE: K-1077
 SOLVENT: Neat
 CONC mg/ml:
 SPECTRUM:
 MONOCHROMATOR SLIT WIDTHS mm 2, 2
 EMISSION MONO.
 ENTRANCE:
 EXIT:
 SLIT SLIDE:
 MULTIPLIER:
 SENSITIVITY:100
 LAMP: Xenon
 CELL TEMP, °C:
 PM TUBE: EMI
 HIGH VOLT, KV:
 DATE: 12/27/77
 OBSERVER: RAV
 Eu_2O_3 - 1.5 mol % (peak 1)
 Sm_2O_3 - 1.0 mol % (peak ?)

Spectrum	Photoem	PMT V
A	1-1	767
B	2-2	737

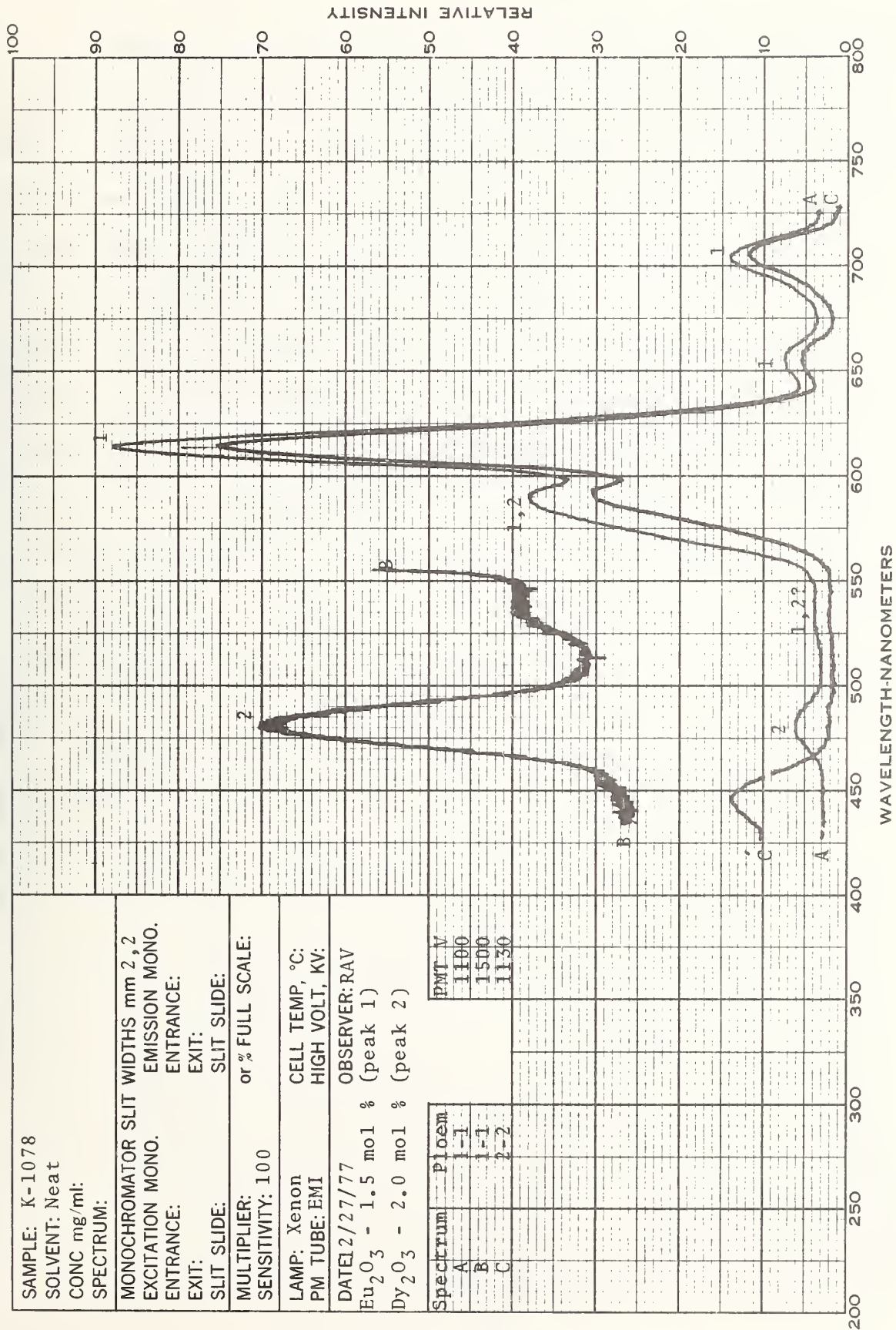


Figure 11. Luminescence spectra of a glass containing Eu₂O₃ and Dy₂O₃.

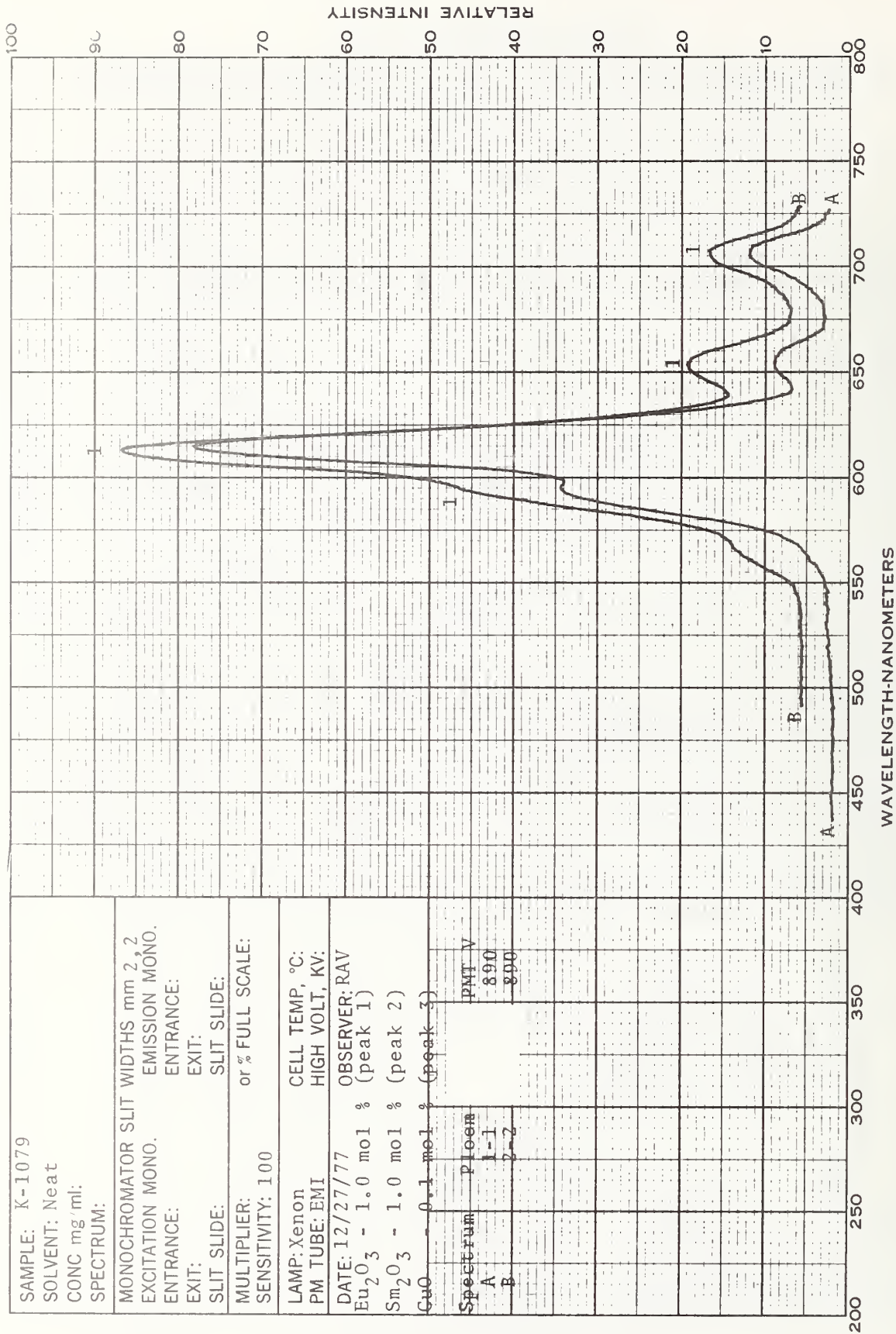


Figure 12. Luminescence spectra of a glass containing Eu₂O₃, Sm₂O₃ and CuO.

OFFICIAL USE ONLY

In summary, one melt, K-1032, containing Tb^{3+} and Sm^{3+} in concentrations of 1.0 mole percent each as the oxides, gives peaks of comparable intensities attributable to the individual ions when excited with radiation passed by a Ploem dichroic mirror-barrier filter combination designated 1-1.

Two additional preliminary melts, designated xxx and yyy in table 1, will be made. Emission spectra will be measured for these materials. Excitation spectra for all melts will be made on the NBS reference spectroradiometer to determine whether an excitation wavelength region can be found which will excite both ions with the resulting emission coming from the individual ions rather than having the energy transfer process occur with consequent strong emission from only one of the ions.

A decision will then be made as to which glass will be used in the final testing. If a decision were to be made at this time, melt K-1032 containing Sm^{3+} and Tb^{3+} would be selected for further work. Using this system as a model, the following work will be done: 1) prepare several melts of varying Sm^{3+} and Tb^{3+} concentration; 2) measure emission spectra; 3) calculate the Tb^{3+} (~ 544 nm)/ Sm^{3+} (~ 602 nm) peak ratios; and 4) obtain precision and accuracy data to determine the smallest ratio difference that could be determined. The particles in

OFFICIAL USE ONLY

these tests would be in the 30-70 μm diameter range, and modification of the detection system to incorporate photon counting may be necessary.

Phase 2. Types of Uniquely Tagged Particles

It is presumed that one might wish to uniquely identify each of a substantial number of secured spaces and, therefore, it would be useful to know to what extent this could be accomplished by the tagged particle technique. There are a number of possible ways to engender unique particulate tags. The simplest is to mix two or more particle types together in known ratios. Among other possibilities are the following:

- o produce single particles with varying ratios of components.
- o coat the particles with unique fluorescent substances.
- o transform the particle shapes from microspheres to aggregates of two, three, four or more microspheres.
- o change the sizes of the microspheres.

There are undoubtedly other possibilities that can be considered, but this project will address only mixtures of components in a single glass microsphere and mixtures of microspheres each of which contain a single component.

Phase 3. Methods of Deployment

A mass of beads with diameters of tens of micrometers pours like a liquid, and can easily be dispersed as a smoke. Such

small particles will adhere to most nonconductive surfaces by electrostatic attraction, but larger particles might not. It might thus be desirable to aspirate them in a "sticky" fluid so that particles of all sizes would adhere to all surfaces [4]. On the other hand, it is important that once attached, the particles should be moderately easy to remove from the surface for two reasons. First, so that the intruder would leave a trail of particulate matter and, secondly, to facilitate decontamination of the guarded space.

Phase 4. Evaluation of the Sensitivity

This ultimate test of the method will be performed for both mixed single-component particles and mixed-component particles. Tests will be made to determine sensitivity to dilution with a known inert particulate material (e.g., polyethylene spheres) and with ordinary dirt. Studies will be made of the statistical technique to be used for searching a collected sample for the unique particles by means of a microscope. From this study one should be able to predict the dilution factor that can be tolerated before detectability is lost. Field tests will be performed at Crane, Indiana [5]. Certain simple tests such as the purposeful addition of particles to shoes and clothing will be made to obtain some feeling for practical sensitivity and the length of time during which one might hope to detect the presence of the unique particles.

OFFICIAL USE ONLY

Countermeasures

Intruders who have set off a Forced Entry Deterrent System (FEDS) will presumably know that everything in sight has been coated with one or more chemicals. They will therefore try to clean themselves and the stolen object as soon as possible. If this is done thoroughly, using the latest clean room technology, there is good likelihood that the trail will end at that point. Evidence will be left in their decontamination chamber for some time (probably weeks) unless the decontamination room itself is decontaminated.

The stolen object should therefore be tagged covertly (e.g., with paint or oil containing the particles), and could even be designed to leave a particulate trail even after rigorous decontamination of the surface. This should produce a successful countermeasure to decontamination. Furthermore, the intruders cannot check the efficiency of their decontamination unless they can match the ultra-high sensitivity of the detection system that is used at NBS [6].

The vehicle used to transport the device will be irreversibly contaminated. Cross contamination by objects contacted by the intruder is very likely. The driver of the vehicle used to move the stolen object away from the area is also likely to be contaminated. In summary, one might liken

OFFICIAL USE ONLY

the process to contamination with an influenza virus. Once it is released, it is very likely to propagate by a number of unforeseen pathways. The only difference is that the virus propagates itself by multiplication [7].

III. INFRARED LASERS FOR TRACE GAS ANALYSIS

The purpose of this project is to investigate the use of lasers for trace gas analysis. It is postulated that a chemical is incorporated into a FDS and is released either separately or together with the particulate tags described in the previous section, covering the secured space and the intruder when the release mechanism is activated. The material slowly releases a given amount of gaseous substance that is then detected by means of the laser radiation.

Detection of the escaped intruder requires the very high sensitivity and selectivity of the laser gas analysis technique. High selectivity is based upon the fact that the taggant gas is made from elements with uniquely defined isotopic ratios; consequently there is little likelihood of finding an identical gas in the environment. This means that the gas analysis system must be able to measure isotopic ratios, e.g., of carbon or oxygen if carbon monoxide or formaldehyde were to be used. Only the gas chromatograph-mass spectrometer (GC-MS) system and

OFFICIAL USE ONLY

the infrared laser seem to have both sufficiently low detection limits and isotope selectivity. The GC-MS is a very slow analysis method compared to the laser spectrophotometric technique. Another interesting potential application of the infrared laser is its use for long path length analysis (to be described in a subsequent section). For these reasons the laser spectroscopic analysis was considered to be the most likely technique for accommodating all of the requirements for this analysis.

Two infrared laser systems have been selected for study: the Stark-modulated CO₂ gas laser system and the semiconductor diode laser system. During phase 1 of this project each system will be evaluated with respect to its performance in fulfilling two requirements of the gas analysis technique: 1) Capability to measure isotopic ratios in simple molecules and 2) adequate limit of detection.

Phase 2 involves performing tests that establish the retention times of various gases absorbed on clothing and skin. Phase 3 will establish the feasibility of the technique under simulated field conditions.

The initial selection of candidate gases will be based upon the results obtained in phase 1 of the project. However, it is suspected that the data obtained in phases 2 and 3 may result

in the selection being based on an iterative process among all three phases of the project.

Phase 1. Establish Limits of Detection and Feasibility of Isotopic Ratio Measurements

Little quantitative work has been published on the measurement of isotope ratios by infrared spectrophotometry, so initial studies have been centered on establishing the capability. Measurements of the naturally-occurring isotope ratios of $^{12}\text{C}/^{13}\text{C}$ in methyl fluoride were made to about 1 percent relative standard deviation with the Stark-modulated CO_2 laser system. Other gases that have been investigated are carbonyl sulfide, formaldehyde, carbon monoxide and methyl mercaptan. While some of these gases meet a few of the tagging system criteria, none meet all of them. Consequently other gases are being considered, including ethyl mercaptan, some of the alkyl disulfides and acetonitrile.

A very important consideration in optimizing the isotopic ratio measurements is the classification of the important segments of the infrared spectrum with respect to mode of vibration and rotation. These assignments can help to determine the energy level that is most intense for each isotope. This could be done by time consuming sweeping of the spectrum experimentally, but among the thousands of lines it

OFFICIAL USE ONLY

would be easy to miss an important region of the spectrum without at least a superficial evaluation of the gas molecule's structure and its effect on the infrared spectrum.

It is very difficult to achieve positive verification of the wavelength of the laser within the resolution of a single peak (0.005 cm^{-1}) in the infrared spectrum. This means that the experiments must identify a set of peaks as being associated with an assigned set of energy levels identified with a structural property within the molecule, just to be assured that the same peak is being measured each time. This mandates theoretical studies involving line assignments. Techniques have been developed for simple molecules and an example of an approach for the formaldehyde molecule is presented in appendix A.

Laser spectroscopy is rapidly becoming the chemical analysis technique with the lowest detection limits [9,10]. Measurements of the limit of detection have proceeded in the direction of establishing background elimination procedures and in the reduction of noise in the system. For the purposes of this study, detection limits will become quantitation limits because sufficient concentration of gas will be needed to measure the isotopic ratio. Phases 2 and 3 have not been

initiated but if phase 1 is successful they are planned to be completed in two more years.

In general the operation of the laser is straightforward and uncomplicated. The electronics are sufficiently well designed, with interlocks that prevent operation at too high a current or temperature. As a result, it is virtually impossible to make an error that damages the laser. Temperature control is stable and easy to achieve, and changing temperatures for tuning purposes is rapid and reproducible. These features make the use of the laser routine.

The tuning characteristics are similar to those described in the literature. That is, as one changes the current at a given temperature, the laser will tune continuously and then jump to another wavelength in a discontinuous fashion. It should be noted, however, that the laser will always operate in the same frequency regions and skip over the same regions, no matter what the temperature. For example, if the laser tunes over $1700-1703 \text{ cm}^{-1}$ and skips to $1705-1708 \text{ cm}^{-1}$ at a particular temperature, skipping over $1703-1705 \text{ cm}^{-1}$, the laser will tune essentially the same way at other operating temperatures and skip over the same regions. Thus, there are "holes" in the tuning curve that cannot be reached with that diode; however, another diode could be fabricated to cover the skipped areas.

OFFICIAL USE ONLY

Reproducibility in day-to-day operation was found to be quite good. That is, returning to the same temperature setting at the same laser current gives the same frequency output.

Formaldehyde

Several spectra of formaldehyde were taken at low pressures. The cell was evacuated and filled to a pressure of 10-20 millitorr with formaldehyde that was obtained by heating paraformaldehyde. The spectra of both the cells and the etalon (interference filter) were taken on successive sweeps under identical laser conditions and recorded together. A typical spectrum is shown in figure 13.

For accurate analysis of the spectra it was considered to be desirable to calibrate the etalon independently of the calibration supplied by the manufacturer. To this end, the etalon was removed from the instrument (although kept in its mount) and its length measured. The length was determined to be $2.59011 \pm .00025$ cm @ 19.8°C , quite close to the 2.5905 cm specified by the manufacturer. Moreover, the flatness was found to be within about 2×10^{-6} cm.

Laser Ranging Chemical Analysis

Long-pathlength atmospheric analysis can be conveniently performed with inexpensive, reliable lasers. This

- The lines are identified as follows:
- 1) $12_0, 12^+13_0, 13^-$
 - 2) $12_1, 12^+13_1, 13^-$
 - 3) $11_1, 10^+12_1, 11^-$
 - 4) $11_2, 9^+12_2, 10^-$
 - 5) $11_3, 8^+12_3, 9^-$
 - 6) $11_8^+12_8$
 - 7) $11_7^+12_7$
 - 8) $11_3, 9^+12_3, 10^-$
 - 9) $11_4^+12_4$ and $11_6^+12_6$
 - 10) $11_5^+12_5$
 - 11) $11_2, 10^+12_2, 11^-$

The oscillating curve is the etalon calibration trace with a spacing between peaks of 0.04783 cm^{-1} .

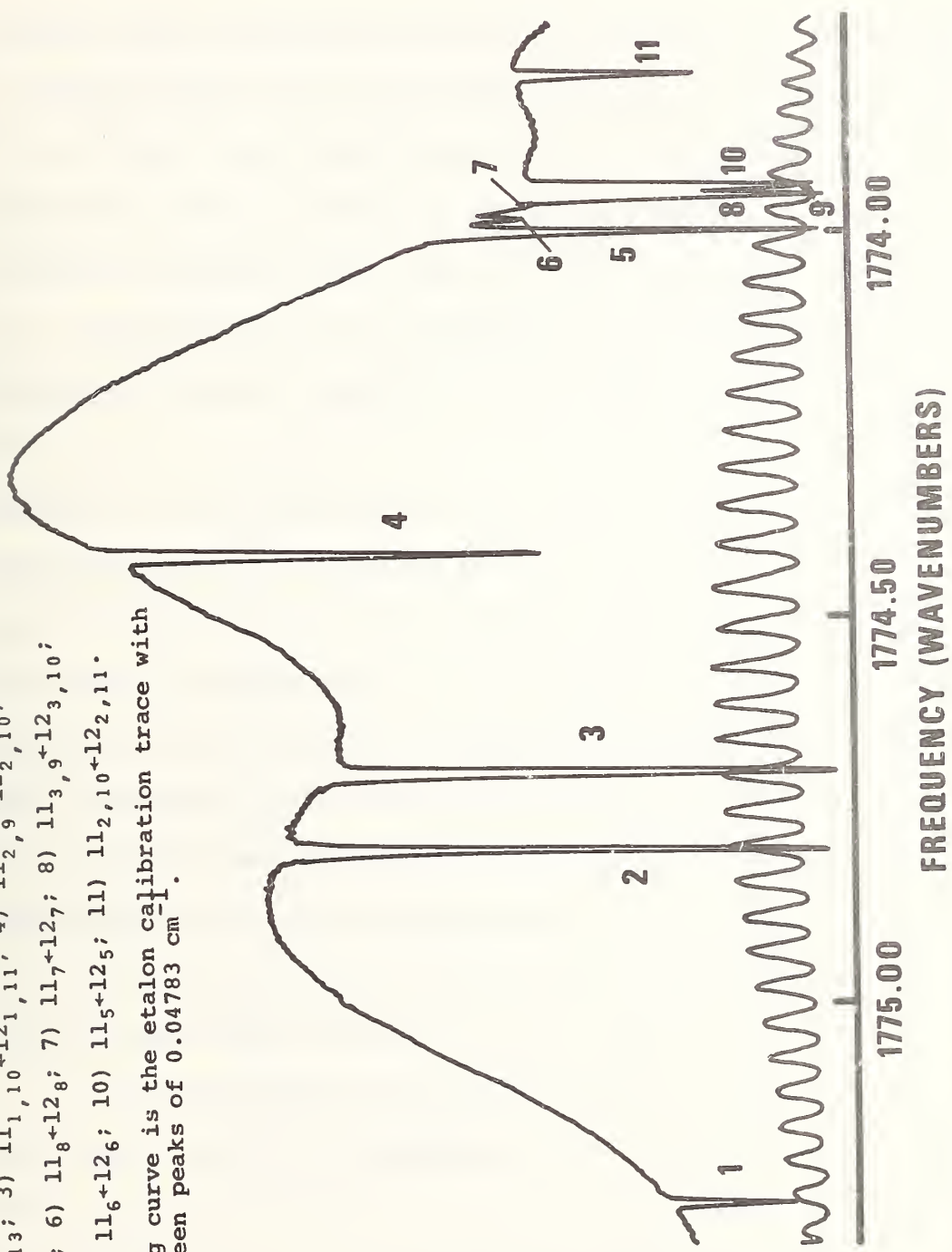


Figure 13. Infrared spectrum of formaldehyde using a semiconductor diode laser.

OFFICIAL USE ONLY

spectrophotometric analysis method uses reflectors that return the beam to a detector located near the laser. This system impacts upon the intruder detection problem in two ways. First, a network of laser beams can be used to cross a secured space. Any object that breaks a beam would trigger an alarm. Second, the same beam can be analyzed for the absorption spectra of the gaseous components in the air within the secured space.

Intruder detection by the beam-break approach is a classic one and much study has been devoted to this type of system by others. As far as is known, however, no one has used the same laser beam for chemical analysis of the atmosphere in the secured space. There are two reasons for doing this: one is an immediate verification that a FEDS had been triggered, and the other is that the existence of poisonous gases can be detected in the event that the intruder attempts to neutralize the guards by introducing them into the atmosphere in the region of the secured space. Such a system might also detect the presence of gases that are damaging to electronic components by determining the composition of exhaust air from the various buildings.

If one assumes that the secure area is about 1 km^2 , it should be possible to detect constituents in the atmosphere at

OFFICIAL USE ONLY

the 100 parts per billion level. The ability to uniquely identify particular constituents in the atmosphere will be impaired as a result of nitrogen (in air) collisional broadening of the infrared molecular transitions. While isotopic ratio analysis could not be performed, the system could transmit an alarm whenever the composition of the atmosphere changed significantly. That is, when certain frequencies that are not characteristic of the normal ambient atmosphere were absorbed, an alarm would sound and further investigation could be made.

Currently, we are thinking about a CO₂ gas laser which emits at some eighty different discrete frequencies. Special optics can be configured to split the laser into a series of beams that would cover the secured space (fig. 14). Reflectors would be situated around the periphery of the secured space, and the returned beam would compare the absorption per unit radiance of the incident laser beam for each of the eighty laser frequencies (fig. 15).

All of this technology is currently available and a prototype could be fabricated in the single beam mode to determine its potential. The gas lasers are commercially available and are known to be very stable with long continuous

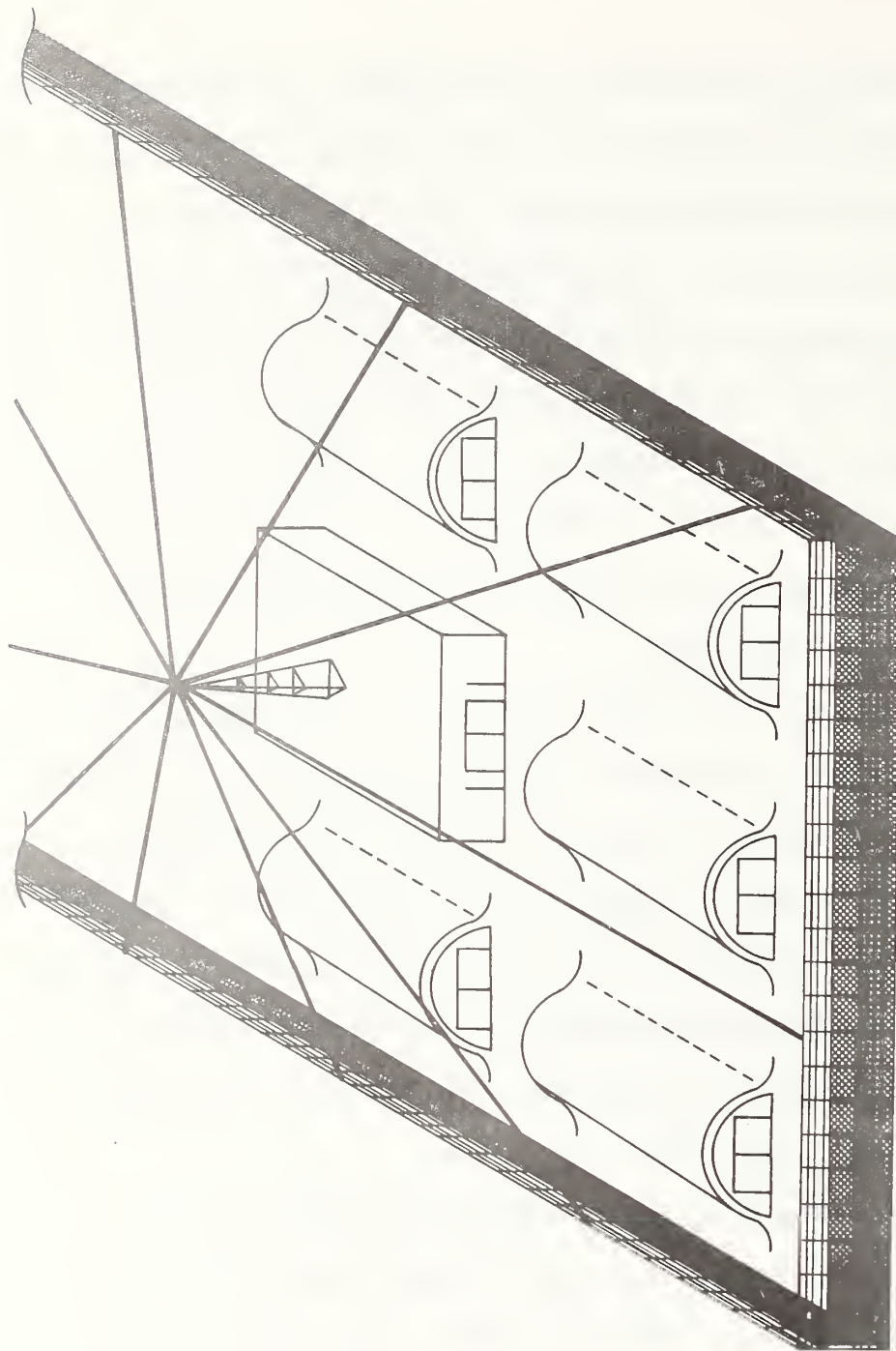


Figure 14. Schematic diagram of laser beam umbrella.

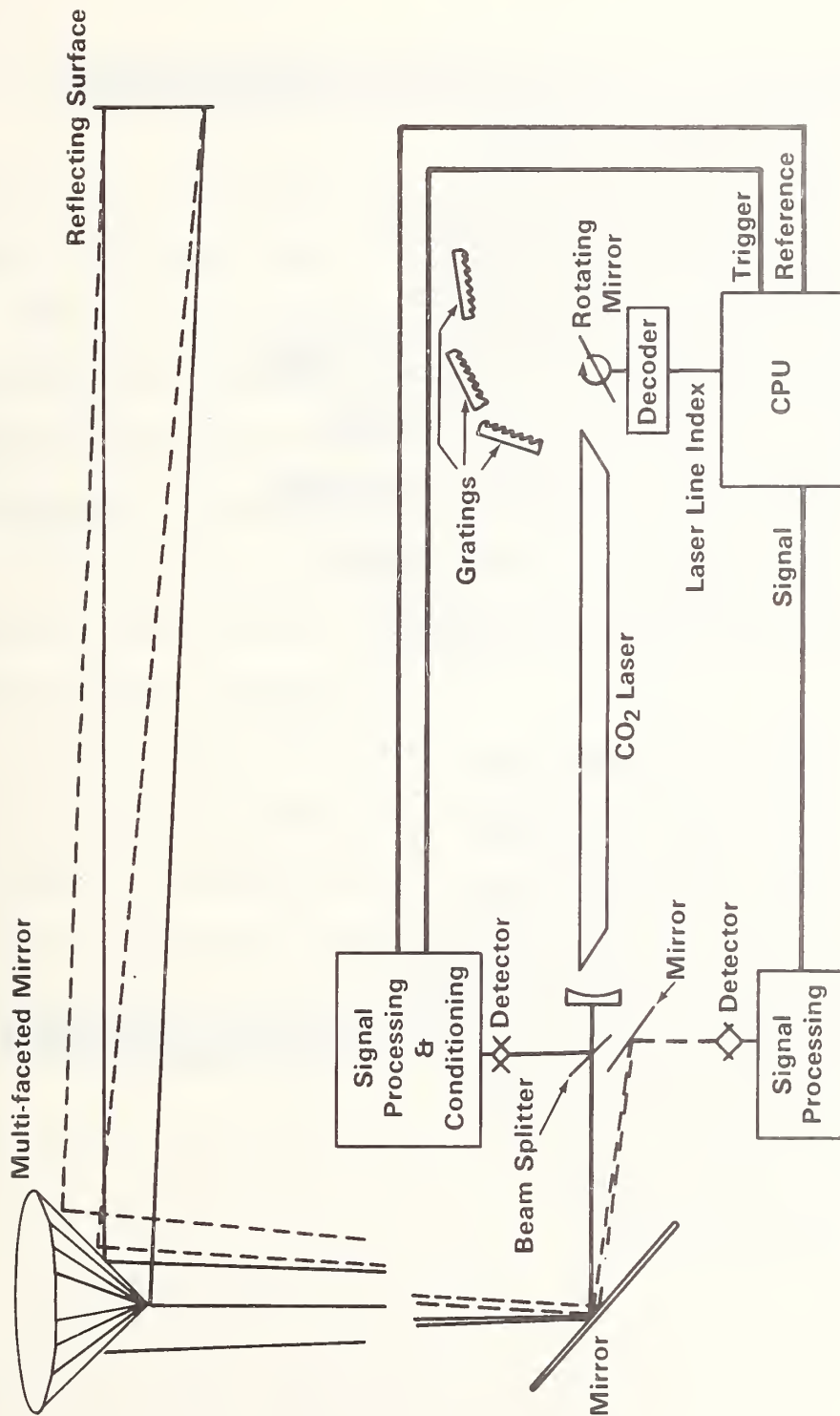


Figure 15. Schematic diagram of laser absorptiometric detection system.

OFFICIAL USE ONLY

operating times at sufficient power. The detector systems are relatively low in cost.

One might obtain data as shown in figure 16. Each of the bars on the graph represent the laser beam intensity returned for a given frequency (designated as R(26), R(24), P(12), etc.). The upper segments of the bars indicate the increases in absorption as a consequence of the introduction of two foreign gases (at concentrations of 1 ppm each) into a normal atmosphere. The absorption characteristics of the two contaminating gases, as well as those of the normal atmosphere, are markedly different at various frequencies. Therefore, one treats the data as a linear combination of uncorrelated components and, by using appropriate computations, can determine an unusual component in the atmosphere. These computations involve pattern recognition techniques which have become quite sophisticated in their ability to distinguish small effects in a complex milieu of other effects.

IV. THE OLFACTORY RECEPTOR AS AN ANALYTICAL INSTRUMENT

We are all aware of the ability of many animals (e.g., bloodhounds) to detect the scent of an escaped prisoner sometimes tens of hours after the trail has been created. Moreover, the scent is uniquely identified with the escaped

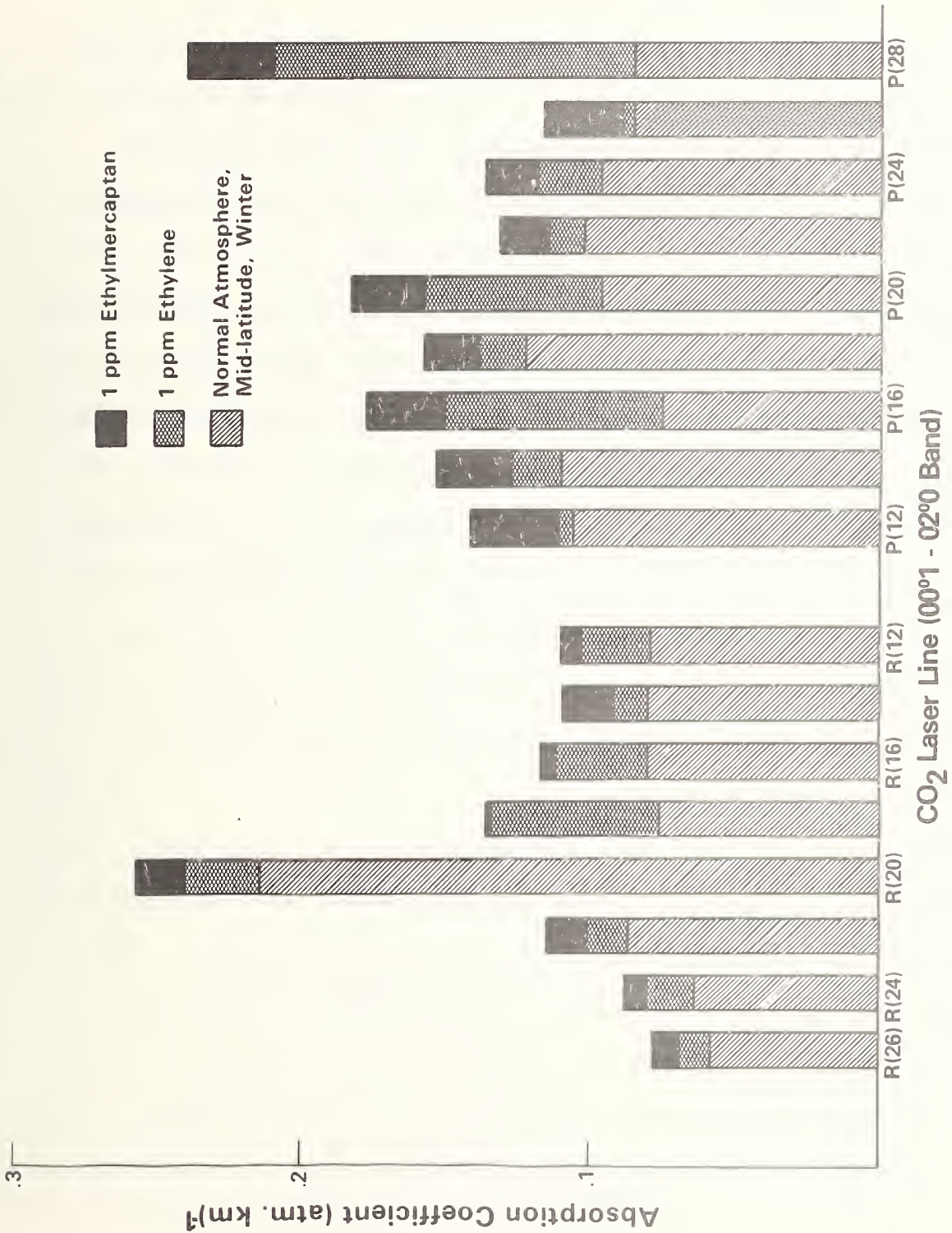


Figure 16. Relative absorption cross sections for a number of the CO₂ infrared laser lines, showing relative contributions due to the ambient atmosphere [16] plus 1 ppm ethylene and 1 ppm ethylmercaptan [15].

OFFICIAL USE ONLY

prisoner and other persons or animals seldom confuse the trail. Obviously, it would be desirable to study this very sensitive and selective olfactory process and to see if a transducer could be developed to make an olfactory analytical instrument possible.

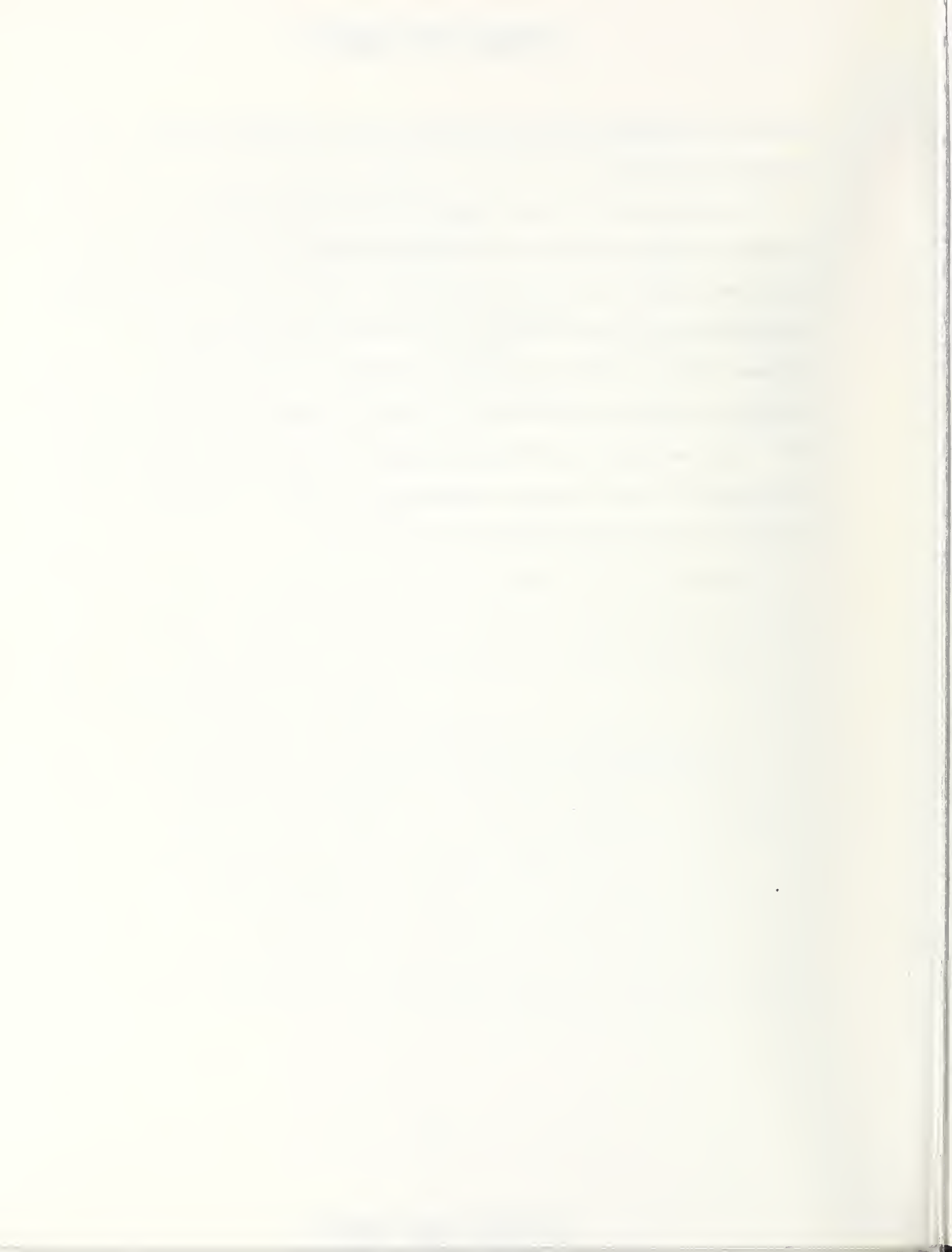
Dr. R. B. Murphy, formerly of the NBS staff and currently a member of the faculty at New York University (Dept. of Chemistry), has written a report on this idea (appendix to ref. [8]) and found that very little work had been done in the field. He did come upon a paper by Fesenko et al. [11] which showed that it is possible to isolate from the epithelium of the frog an active substance that is capable of sensitizing a lipid bilayer to the presence of an odor. The response to the odor can be seen through the measurement of the electrical resistance across the bilayer.

In December 1977, Dr. Murphy succeeded in obtaining a separation on Sephadex G-200 of a substance with a molecular weight of about 330,000 [14]. The olfactory activity of the material was measured by exposing the material to n-butyl disulfide. Spectrophotometric absorbance at 215 nm showed a linear-log response in two ranges from 10^{-7} to 10^{-10} molar and 10^{-10} to 10^{-11} molar [12]. From these data, it is clear that a

OFFICIAL USE ONLY

measurable response can be obtained from extremely small amounts of odorant.

The major task is to understand how selectivity is obtained. This requires an understanding of the biochemistry associated with the olfactory process. This study is currently in progress at NYU (though at a relatively slow pace) and a minimum effort is being made with respect to producing a transducer that might be used to make an analytical instrument [13]. The potential of this technique is extremely great and considerable effort must be expended in order to realize the goal of an olfactory analytical instrument.



OFFICIAL USE ONLY

References and Notes

1. A demonstration was given in Washington, D.C. of the use of particle tagging materials in explosives. Particles were formulated in colored fluorescent layers by 3M Corp. and ceramic spheres coated with a fluorescent substance were fabricated by Westinghouse Co. for the Aerospace Corp. The particles used in these tests were large but could possibly be made useful for this application as well.
2. a) Velapoldi, R. A., J. Res. Nat. Bur. Stand. 76A, No. 6, 641 (1972); b) Reisfeld, R., *ibid*, 613 (1972); c) Velapoldi, R. A., Reisfeld, R., and Boehm, L., Phys. Chem. of Glass 14, 101 (1973); d) Reisfeld, R., Velapoldi, R. A., and Boehm, L., J. Phys. Chem. 76, 1293 (1972); e) Velapoldi, R. A., Travis, J. C., Cassatt, W. A., and Yap, W. T., J. Microscopy 103, 293 (1975).
3. Dr. M. F. Dilmore, Inorganic Glass Section, NBS.
4. Magnetic particles have been made to enhance their attachment to iron surfaces. See reference 1.
5. R. M. Henry and D. D. Olson. Fleet Logistic Support Department and Applied Sciences Department, Naval Weapons Support Center, Crane, Indiana 47522.
6. Other particle detection systems can be devised that would make the problem even more intractable. For example Raman spectra can be taken of particles as small as 1 μm .
7. On the other hand, many die in hostile environments; presumably the ceramic particles do not.
8. J. R. DeVoe, "Intruder Detection by Chemical Analysis," Internal report submitted to the Law Enforcement Standards Laboratory, NBS and the Defense Nuclear Agency, DOD.
9. While recent literature reports detection of single atoms (Science 199 1191-3 (1978)) none of these methods can be applied to practical samples such as air analysis. Work in our group has demonstrated practical detection limits that are very low for solution analysis using dye lasers and molecular gas analysis using infrared lasers.

OFFICIAL USE ONLY

10. D. M. Sweger and J. C. Travis, to be published.
11. Fesenko, E. E., Novoselov, V. I., Pervukbin, G. Ya., and Fesenko, N. K., Biochem. Biophys. Acta 466 347-56 (1977).
12. Murphy, R. B., Cho, J., and Loxer, J., "Isolation of an Olfactory Receptor Sensitive to Subnanomolar Odorant Concentrations," to be published.
13. Some work is being carried out at NYU to determine the best method to render the active protein insoluble.
14. Recent data obtained by R. B. Murphy show that the separated fraction contains a mixture of at least 16 different proteins.
15. Moyer, A., Comera, J., Charpentier, H., Jassored, C., Applied Optics 17 391-2 (1978).
16. Kelley, P. L., McClatchey, R. A., Long, R. K., Nelson, A. S., Optical and Quantum Electronics 8 117-144 (1976).

Appendix A--ASSIGNMENT OF VIBRATION-ROTATION
ENERGY LEVELS IN FORMALDEHYDE

In the infrared region of the electromagnetic spectrum, molecules absorb radiation by going from one vibrational state to another. These vibrational states can be decomposed into normal modes of vibration of the constituents and are quantized with a quantum number, ν . When the three degrees of freedom each for translational and rotational motion are eliminated, there are $3N-6$ (where N is the number of atoms), degrees of freedom remaining; and thus $3N-6$ normal modes of vibration. All molecular vibrations are multiples and/or combinations of these modes. Within any particular normal vibrational mode there is a set of energy levels that arise from the rotational energy of the molecule. In general, these rotational levels are spaced much closer together in energy than are the vibrational modes, so that transitions between rotational levels appear as structure in vibrational bands. The quantum number associated with the rotation in a molecule is labeled J , and transitions are allowed for which $\Delta\nu=1$ and $\Delta J=0, \pm 1$. The structure that is observed on infrared bands is classified as P, Q or R branches corresponding to transitions for which $\Delta J=-1, 0$ and $+1$, respectively, where $\Delta J=J'-J''$ [see eq. (12)]. Each branch consists of a series of narrow absorption lines that

OFFICIAL USE ONLY

arise from transitions originating from the various rotational energy levels and are labeled by the value of J in the lower vibrational state (usually the ground state). In a low resolution infrared spectrum this detailed structure is blended together, but in medium or high resolution spectra it is often clearly evident. Figure A1 [8] is a medium resolution spectrum of an uncomplicated band of methyl fluoride and illustrates the vibrational-rotational structure.

The infrared spectrum of formaldehyde has been studied in detail by several researchers [1-7,9]. Since there are four atoms there are $(3N-6)=6$ normal modes of vibration, as illustrated in figure A2 [11]. This figure includes the mode numbering and the frequencies of the modes.

Figure A3 shows the region of the infrared spectrum of formaldehyde that overlaps with the CO₂ laser emission lines [9]. While this is a complicated spectrum it can be successfully treated in terms of a strong Coriolis interaction between the two modes ν_4 and ν_6 which causes perturbation on the structure of these vibrations. Coriolis forces are mechanical forces introduced as a result of the interaction of linear motion (vibration) and rotation and are of the form

$$\vec{F}_c = 2m\vec{v} \times \vec{\omega} \quad (1)$$

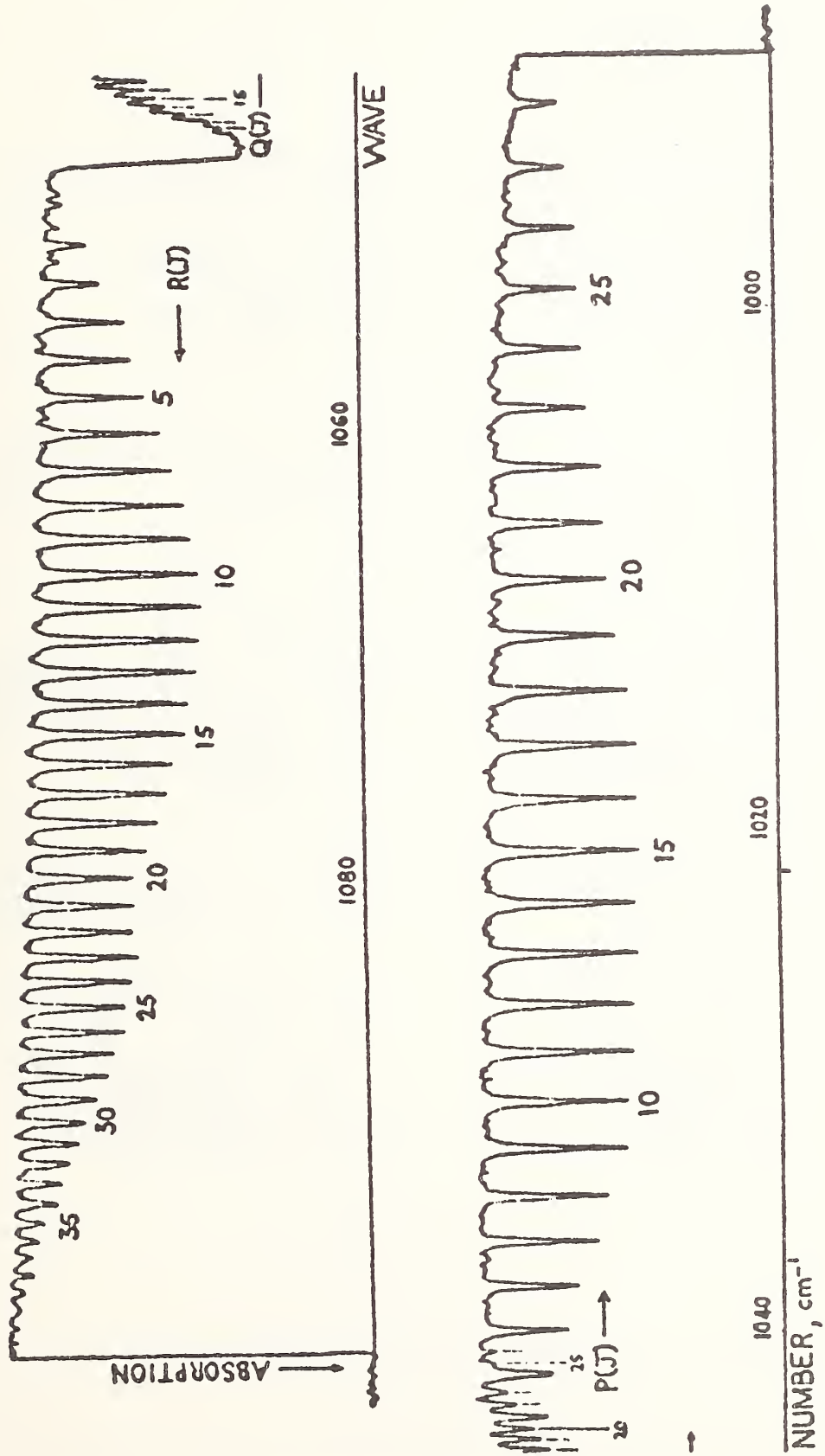


Figure A1. Infrared absorption spectrum of CH_3F .

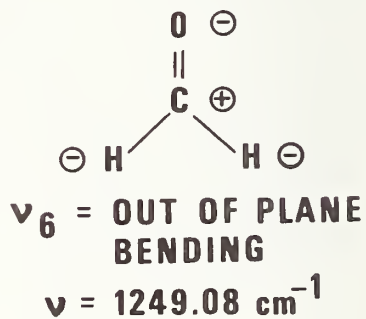
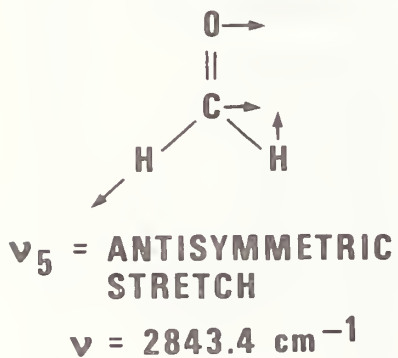
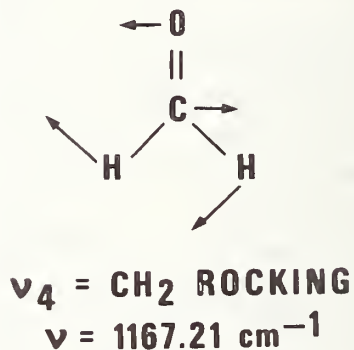
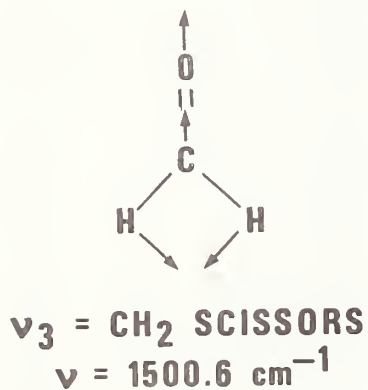
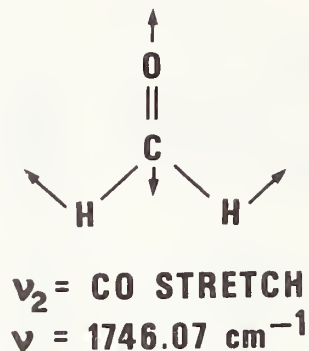
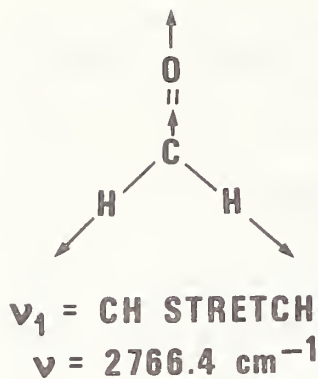


Figure A2. Fundamental modes of formaldehyde.

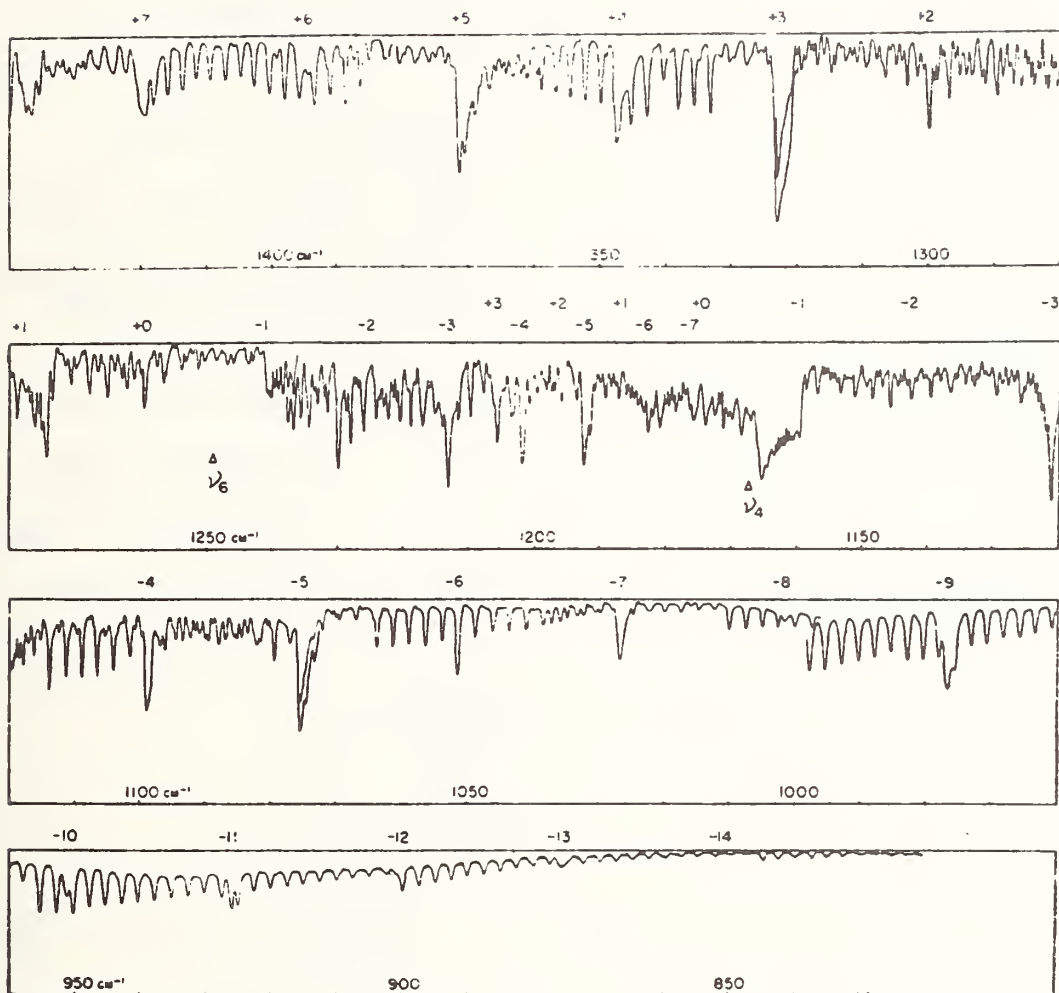


Figure A3. Infrared absorption spectrum of formaldehyde.

OFFICIAL USE ONLY

where v is the linear velocity of the vibrating atoms and ω is the angular velocity of rotation. These forces can give rise to other apparent vibrational modes in the molecule and are illustrated for H_2CO in figure A4. If the induced vibration is close in energy to the initial vibration, a resonance interaction can occur. The Coriolis resonance will both shift the positions of the lines and alter relative intensities, making the spectrum difficult to analyze.

In general any analysis of Coriolis interaction in an asymmetric rotor is extremely complex and requires large amounts of computation. However, the problem can be simplified for formaldehyde by assuming that it is a symmetric rotor. A measure of the asymmetry of the molecule can be obtained by Ray's asymmetry parameter [10] given by

$$K = \frac{2B-A-C}{A-C}$$

where A , B and C are the rotational constants and are defined as

$$A = \frac{h}{2\pi^2 c I_A}, \quad B = \frac{h}{2\pi^2 c I_B}, \quad C = \frac{h}{2\pi^2 c I_C},$$

I_A , I_B and I_C are the moments of inertia about the three principal axes, h is Planck's constant, and c is the velocity of light. The rotational constants are ordered so that $A \geq B \geq C$. Thus the asymmetry parameter becomes -1 for a prolate symmetric top ($B=C$) and $+1$ for an oblate symmetric top ($A=B$). In the

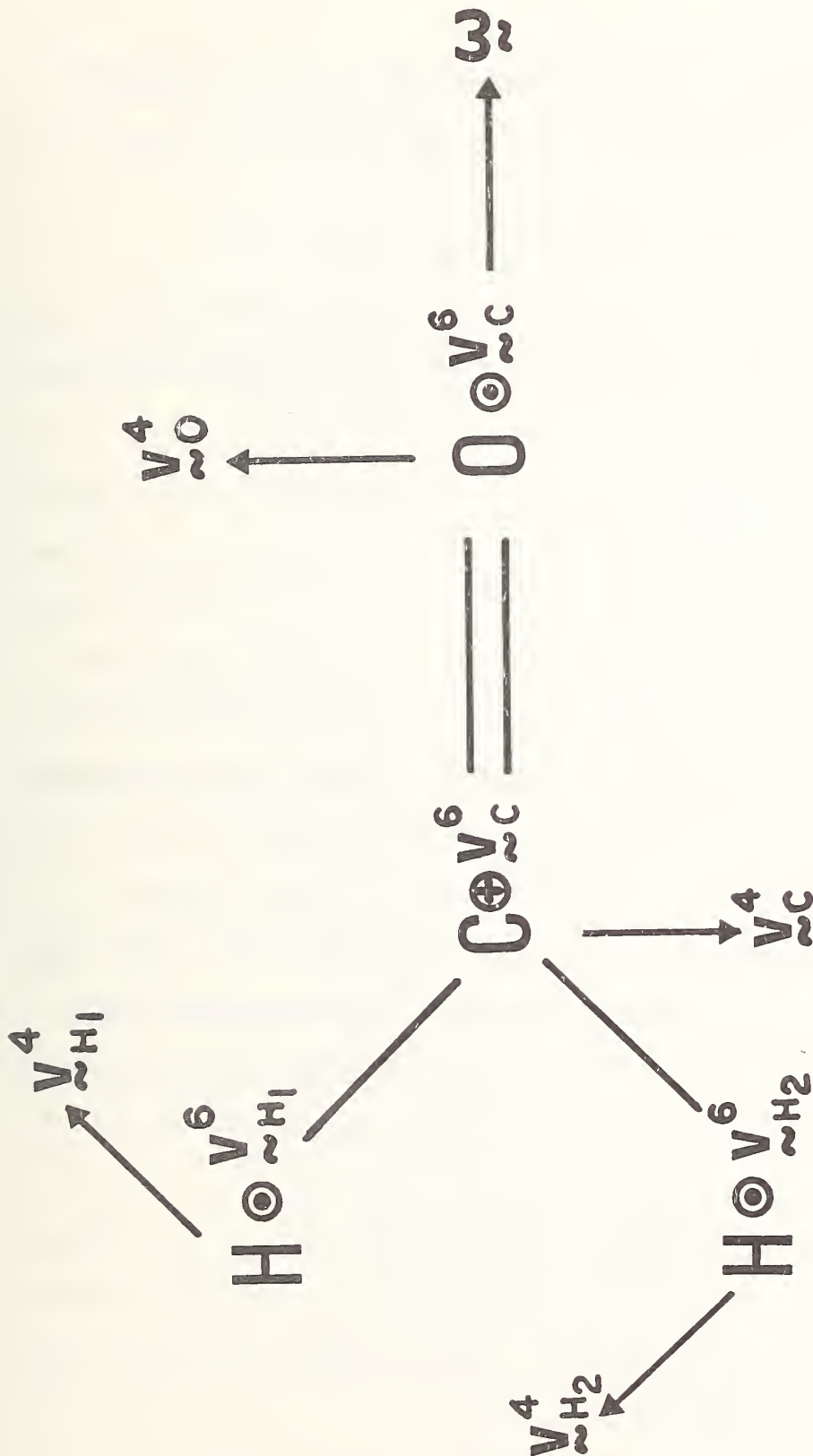


Figure A4. Depiction of Coriolis interaction in formaldehyde. The ν_4 vibrational mode induces the ν_0 mode through the Coriolis interaction given by $2m v_{xw}$. The symbols θ and 0 represent vectors out of and into the page, respectively, while the superscripts indicate the vibrational band associated with that vector.

OFFICIAL USE ONLY

case of formaldehyde, the equilibrium values are $A=9.5795\text{cm}^{-1}$, $B=1.3033\text{cm}^{-1}$ and $C=1.1462\text{cm}^{-1}$ giving [4]

$$K = -.9627$$

which is quite close to -1. Another parameter that is especially useful for a slightly asymmetric prolate rotor is [10]

$$b_p = \frac{C-B}{2A-B-C} = \frac{K+1}{K-3} = (-0.0094) \quad (3)$$

This parameter is zero for a symmetric top and increases in magnitude as the asymmetry increases. One other condition needs to be evaluated concerning the accuracy in assuming a symmetric top. For an asymmetric top, as well as a symmetric top, the total angular momentum J and its projection M_J on an axis fixed in space are considered valid quantum numbers.

However, in an asymmetric rotor the projection of J onto the molecular axis of symmetry, K is not a valid quantum number. Thus any attempt to use K is an approximation. Townes and Schawlow, for a slightly asymmetric top, suggest substituting

$$W = K^2 + c_1 \frac{b}{p} + c_2 \frac{b^2}{p^2} + c_3 \frac{b^3}{p^3} + \dots \quad (4)$$

and they have tabulated the coefficients c_i . However, since b is so small and K is relatively large in this treatment, this correction will be ignored.

OFFICIAL USE ONLY

In the symmetric top approximation, the unperturbed energy levels are written as [3]

$$E_i^0(J,K) = \nu_i + (A_i - \bar{B}_i)K^2 + \bar{B}_i J(J+1) \quad (5)$$

where $\bar{B} = \frac{1}{2}(B+C)$ and ν_i is the frequency of band origin. An absorption will take place between two such levels in different ν_i 's. The Coriolis interaction between ν_4 and ν_6 can be included as a perturbation, where the differences (in frequency) between identical rotational levels in ν_4 and ν_6 is [3,9]

$$\Delta_{6,4}^0(K) = E_6^0(J,K) - E_4^0(J,K) = \nu_6 - \nu_4 + \left[(A_6 - B_6) - (A_4 - B_4) \right] K^2 \quad (6)$$

The off-diagonal matrix element in the perturbation is

$$H_{6,4} = \xi_{6,4}^\alpha K \quad (7)$$

where $\xi_{6,4}^\alpha$ is called the Coriolis interaction parameter [3,9].

By solving the secular determinant, the perturbed energy levels are obtained as

$$E'_{6,4}(J,K) = E_{6,4}^0(J,K) \pm \frac{1}{2} \left[\Delta_{6,4}^1(K) - \Delta_{6,4}^0(K) \right] \quad (8)$$

$$\text{where } \Delta_{6,4}^1(K) = \left[\left(\Delta_{6,4}^0(K) \right)^2 + 4 \left(\xi_{6,4}^\alpha K \right)^2 \right]^{1/2} \quad (9)$$

The Stark Effect

The rotational spectrum of a molecule may be expected to be modified when the molecule is placed into an electric field, since the field exerts a torque on the dipole moment and thereby effects its rotational motion. A particular rotational energy level, J , is thus split into $(2J+1)$ sublevels given by $M_J = -J, -J+1, \dots, J$. When the interaction of the field with the molecule is calculated by the use of quantum mechanical perturbation theory, two primary cases emerge. These are the so-called "first-order" and "second-order" Stark effects, which derive their names from the type of perturbation approximation that is the dominant contribution to the energy levels in the molecule. The first-order Stark effect occurs in molecules described as symmetric-top rotors, linear molecules under certain conditions and some slightly asymmetric rotors. The second-order Stark effect is much more complex, involving effects of many interacting levels. Fortunately, formaldehyde is sufficiently close to being a symmetric top that the first-order theory is sufficient.

For a symmetric top the interaction Hamiltonian H for an external electric field, E , and an electric dipole moment, μ , is

$$H = -\underline{\mu} \cdot \underline{E} \quad (10)$$

OFFICIAL USE ONLY

This results in a term value of

$$W = - \frac{MK}{J(J+1)} \mu E \quad (11)$$

Then, for a vibrational-rotational transition, the shift in frequency is

$$W'-W'' = \Delta\nu = - \left\{ \mu' \frac{M'K'}{J'(J'+1)} - \frac{M''K''}{J''(J''+1)} \right\} E \quad (12)$$

where the prime denotes the upper state and double prime the lower state. Absorption takes place when $\Delta\nu = \nu_{\text{laser}} - \nu_J$, so that as E is increased, various M components of the absorption line are brought into coincidence with the laser. Defining $\Delta M = M' - M''$, we can rewrite the equation as:

$$\frac{1}{E} = - \frac{1}{\Delta\nu} \left\{ M'' \left[\frac{\mu'K'}{J'(J'+1)} - \frac{\mu''K''}{J''(J''+1)} \right] + \Delta M \frac{\mu'K'}{J' * J'+1} \right\} \quad (13)$$

Notice that a plot of $1/E$ vs. M'' will yield a straight line.

The values of ΔM are determined by the polarization of the absorbed photons with respect to the external electric field. If the electric field of the photons is parallel to the external field, the only allowed transitions are those for which $\Delta M=0$. Likewise, for the perpendicular case the only allowed transitions are those for which $\Delta M=\pm 1$. While eq. (13) is quite general, it is useful to rewrite it for particular cases.

OFFICIAL USE ONLY

$\Delta M=0$

For $\Delta M=0$ the intercept term is zero and the straight line passes through the origin. This is very useful for identification of the J quantum number when there are no other guidelines. One merely starts with an arbitrary number for M''_{\max} (which must be an integer), plots $1/E$ vs. M'' and adjusts the value of M''_{\max} until the line passes through the origin. The slope of the line is different, depending upon whether the absorption is in a P, Q or R branch, so these will each be considered separately.

A. P-branch: $J' = J'' - 1$

$$\begin{aligned} 1/E &= - \left(\frac{\mu_0}{\Delta v} \right) \frac{M}{J''(J''+1)(J''-1)} \left[(J''+1)K' - (J''-1)K'' \right] = \\ &= - \left(\frac{\mu_0}{\Delta v} \right) \frac{M''K''}{J''(J''+1)} \left[\frac{(J''+1)K'}{(J''-1)K''} \right] - 1 \end{aligned} \quad (14)$$

where it is assumed that the dipole moment is the same for upper and lower states. If this is not the case one simply converts all K'' to $\mu''K''$ and K' to $\mu'K'$ and deletes μ_0 .

B. Q-branch: $J' = J''$

$$\frac{1}{E} = - \left(\frac{\mu_0}{\Delta v} \right) \frac{M''}{J''(J''+1)} [K' - K''] = - \left(\frac{\mu_0}{\Delta v} \right) \frac{K''M''}{J''(J''+1)} \left(\frac{K'}{K''} - 1 \right) \quad (15)$$

C. R-branch: $J'+J''+1$

$$\begin{aligned} \frac{1}{E} &= - \left(\frac{\mu_0}{\Delta v} \right) \frac{M''}{J''(J''+1)(J''+2)} \left[J''K' - (J''+2)K'' \right] \\ &= - \left(\frac{\mu}{\Delta v} \right) \frac{M''K''}{J''(J''+1)} \left[\frac{J''}{(J''+2)} \frac{K'}{K''} - 1 \right] \end{aligned} \quad (16)$$

$\Delta M=+1$

In the case where the polarization is perpendicular to the field, the slope remains the same as in the previous case. However, it is possible to obtain more information about the line assignment by considering the ratio of the slope to intercept. This ratio has the advantage of eliminating Δv , which is generally unknown. Thus only $\mu'K'$, $\mu''K''$ and J'' remain, the latter of which is known from M''_{\max} in the previous section. This leaves only $\mu'K'$ and $\mu''K''$ which can in general be deduced from the slope/intercept. Again, consider the three cases.

A. P-branch: $(J'=J''-1)$

$$\frac{1}{E} = - \left(\frac{\mu_0}{\Delta v} \right) \frac{1}{J''(J''+1)} \left\{ M''K'' \left[\frac{(J''+1)K'}{(J''-1)K''} - 1 \right] + \Delta MK' \frac{J''+1}{J''-1} \right\} \quad (17)$$

$$\left| \frac{\text{slope}}{\text{intercept}} \right| = \left| \frac{K'}{\Delta M} \left(\frac{J''+1}{J''-1} \right) \left(1 - \frac{J''-1}{J''+1} \frac{K'}{K''} \right) \right| \quad (18)$$

Note that the sign is indeterminate until the sign of ΔM is known.

OFFICIAL USE ONLY

B. Q-branch: $(J' - J'')$

$$\frac{1}{E} = - \left(\frac{\mu_0}{\Delta v} \right) \frac{1}{J''(J''+1)} \left[M''K'' \left(\frac{K'}{K''} - 1 \right) + \Delta M K' \right] \quad (19)$$

$$\left| \frac{\text{slope}}{\text{intercept}} \right| = \left| \frac{K' - K''}{K' \Delta M} \right|$$

C. R-branch: $(J' = J'' + 1)$

$$\frac{1}{E} = - \left(\frac{\mu_0}{\Delta v} \right) \frac{1}{J''(J''+1)} \left\{ M''K'' \left[\left(\frac{J''}{J''+2} \right) \frac{K'}{K''} - 1 \right] + \frac{\Delta M J'' K'}{J''+2} \right\} \quad (21)$$

$$\left| \frac{\text{slope}}{\text{intercept}} \right| = \left| \frac{1}{\Delta M} \frac{J'' K'}{J''+2} \left[1 - \frac{J''+2}{J''} \frac{K''}{K'} \right] \right| \quad (22)$$

One additional parameter that is useful for making line identifications is the relative intensities for successive lines in a J multiplet. For $\Delta M = 0$ these are given below:

$$\text{R-branch: } I_m \propto \left[(J+1)^2 - M^2 \right] \left[(J+1)^2 - K^2 \right] / (J+1)^2 (2J+1) (2J+3) \quad (23)$$

$$\text{P-branch: } I_m \propto \left[J^2 - M^2 \right] \left[J^2 - K^2 \right] / J^2 (2J+1) (2J-1) \quad (24)$$

$$\text{Q-branch: } I_m \propto M^2 K^2 / J^2 (J+1)^2 \quad (25)$$

Note that for both P and R branches the intensity decreases with increasing M and zero for $M=J$ in the P branch, while the opposite is true for the Q branch transitions. For $\Delta M = \pm 1$ the intensity pattern is the reverse, so it is relatively easy to identify Q-branch lines on the basis of intensity.

OFFICIAL USE ONLY

Experimental

A schematic outline of the experimental apparatus is shown in figure A5. The laser is a non-commercial CO₂, flowing gas laser with a cavity length of 1 meter and active discharge length of approximately 65 cm. Laser line selection is done by means of a 2.5 cm diameter, 75 lines per mm grating blazed for 10.5 μm. A ZnSe 90 percent reflecting mirror, with a 2m radius of curvature, is used as the output coupler, and at least 75 lines can be observed with sufficient intensity for spectroscopy. Irises are mounted at both ends of the cavity to confine the laser modes and provide some control on the power output. The laser frequency is stabilized onto the peak of the gain curve by sinusoidally modulating the cavity length via a piezoelectric translator (PZT) and using feedback techniques.

At the heart of the system is the Stark cell, which consists of two parallel stainless steel electrodes inside a vacuum chamber, as shown in figure A6. The electrodes are 40 cm x 6.3 cm x 2.5 cm and are maintained at a precise spacing by precision ground quartz spacers. Electrical connections to the plates are made via high voltage vacuum feedthroughs. One plate is connected to the output of a high voltage operational power supply in which 9 kHz sine wave modulation, triangular wave sweep and DC offset voltages are summed and amplified.

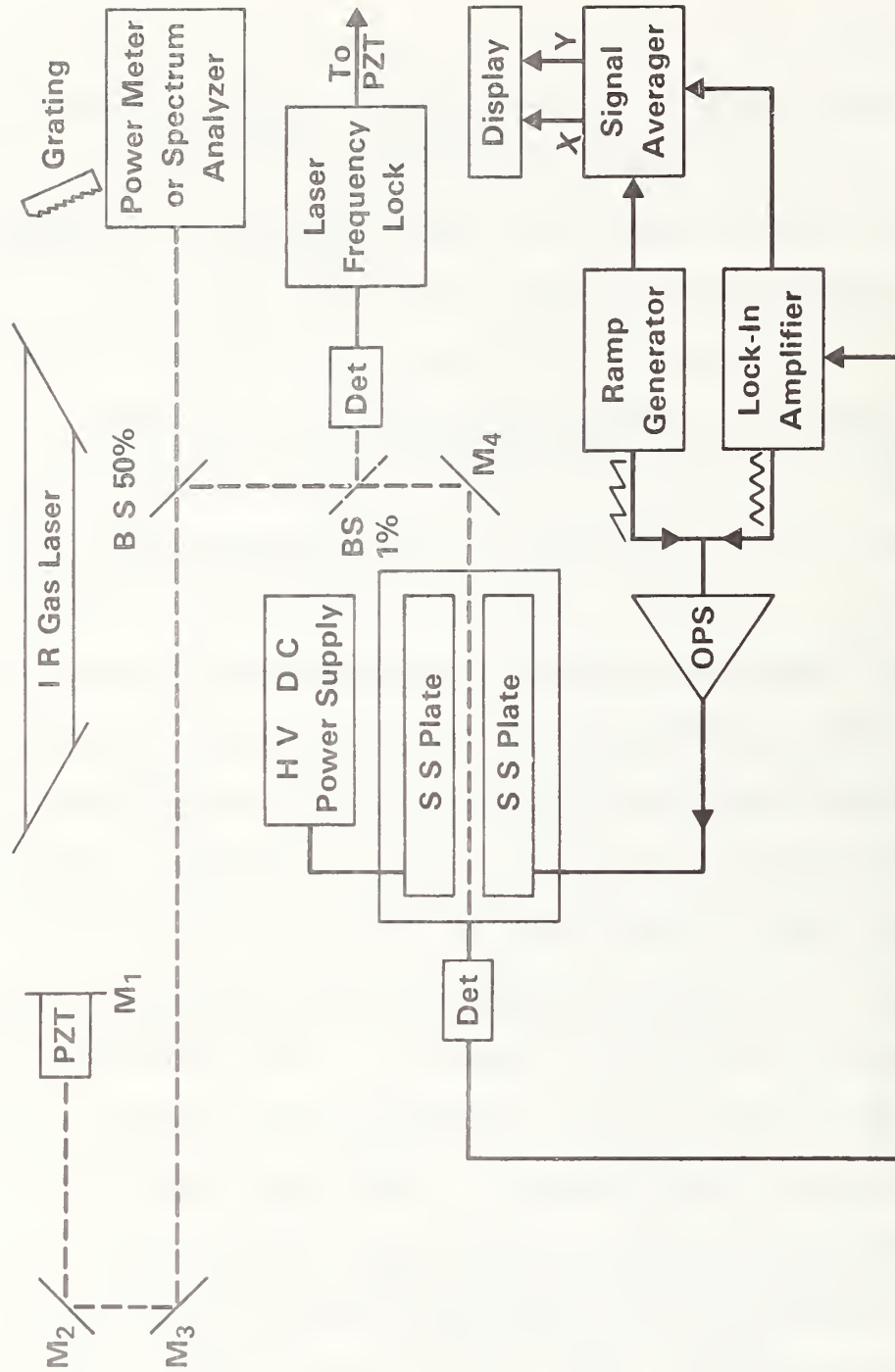


Figure A5. Schematic diagram of laser Stark scanning apparatus.

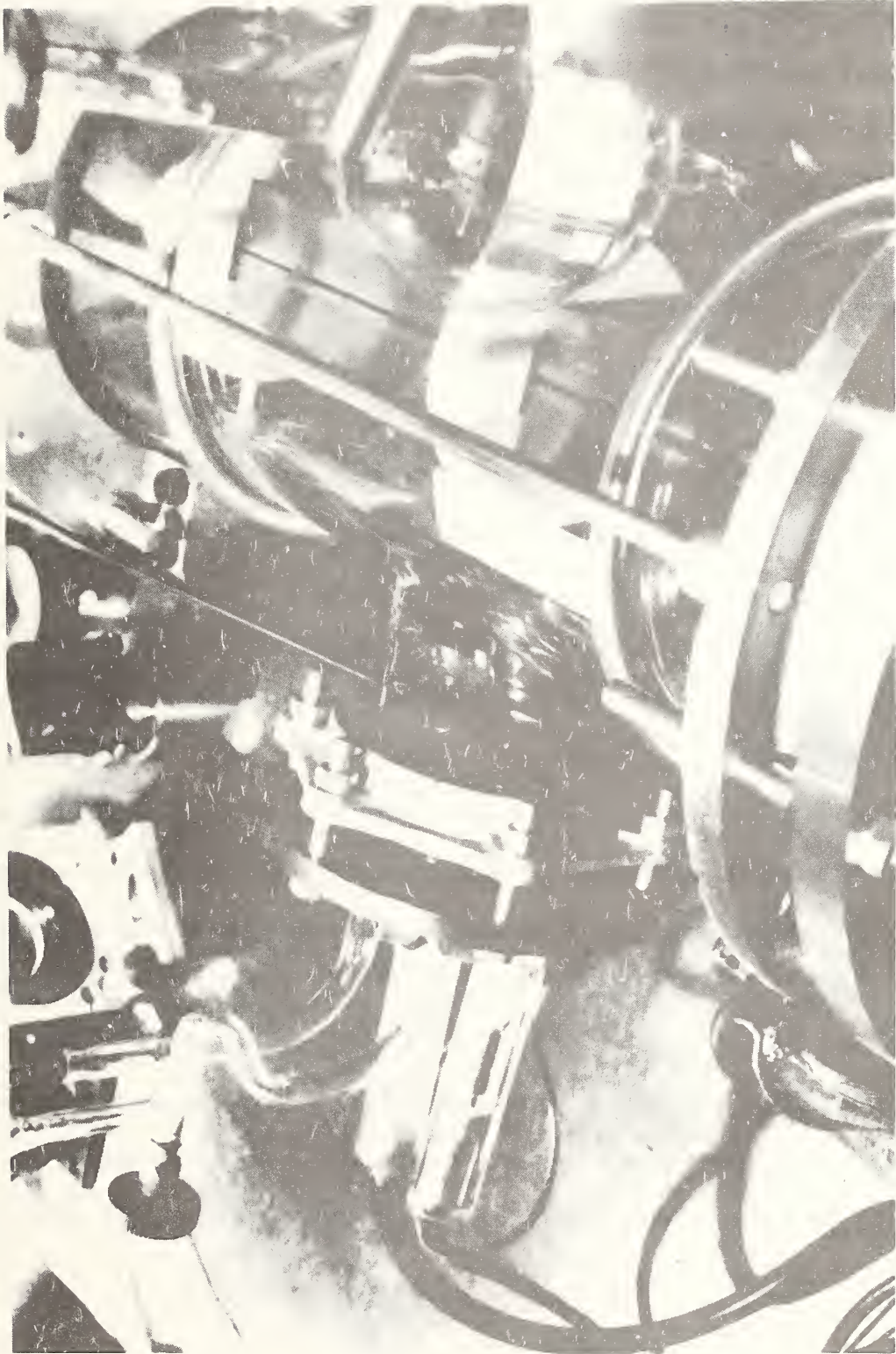


Figure A6. Sample cell for Stark spectroscopy.

OFFICIAL USE ONLY

The other plate is connected to a DC high voltage power supply to provide additional bias of up to 5 kV, so that fields as high as 100 kV/cm can be generated.

In practice, electrical breakdown occurs above 70 kV/cm, depending upon the internal gas pressure, so data were seldom taken above 60 kV/cm. As a practical consideration data were taken in sweeps covering 19 kV/cm with an overlap of 1 kV/cm between successive sweeps, i.e., 0-19 kV/cm, 18-37 kV/cm, etc. The spectra were recorded on graph paper with voltage markers for calibration, and the peak positions were read from the charts. Sample charts are shown in figures A7 and A8. While there are more accurate techniques for measuring peak positions, they are time consuming and were judged to be unnecessary for this work.

Formaldehyde monomer was formed by evacuating a small vial containing paraformaldehyde, sealing off the vacuum pump and heating the vial until the pressure rose to 50-100 millitorr. No further steps were taken to purify the formaldehyde before filling the Stark cell. The fill pressure in the cell was approximately 5 millitorr as measured by a thermocouple gauge located on the vacuum flange of the cell. At this pressure, room temperature polymerization and absorption on the walls of the vacuum chamber are avoided.

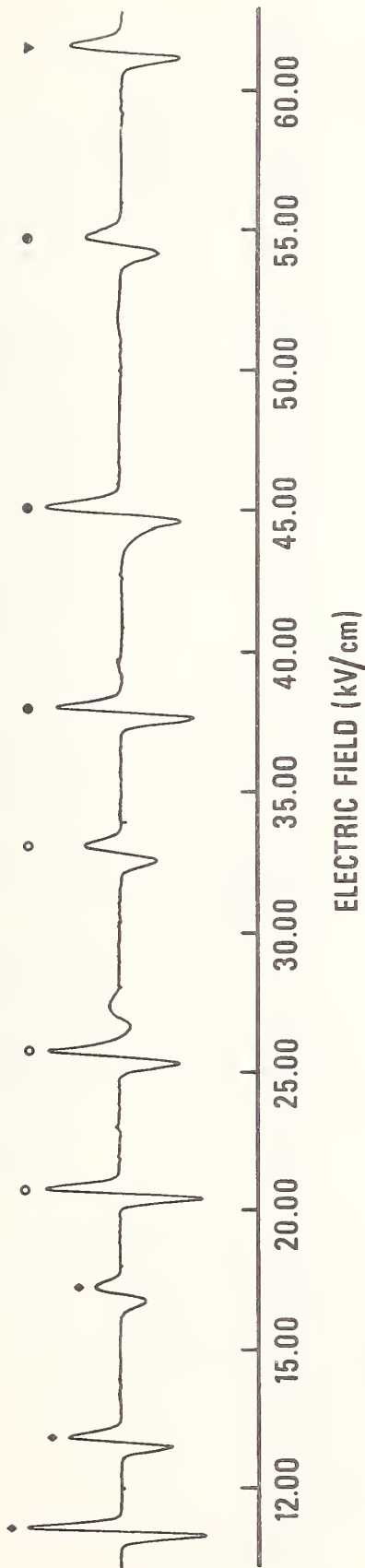


Figure A7. Stark spectrum for formaldehyde taken on the R(16), 9.6 μm , laser line. The symbols identify M_J components of the following lines: ●:J=7; V:J=8; ○:J=5; ◊:J=6.

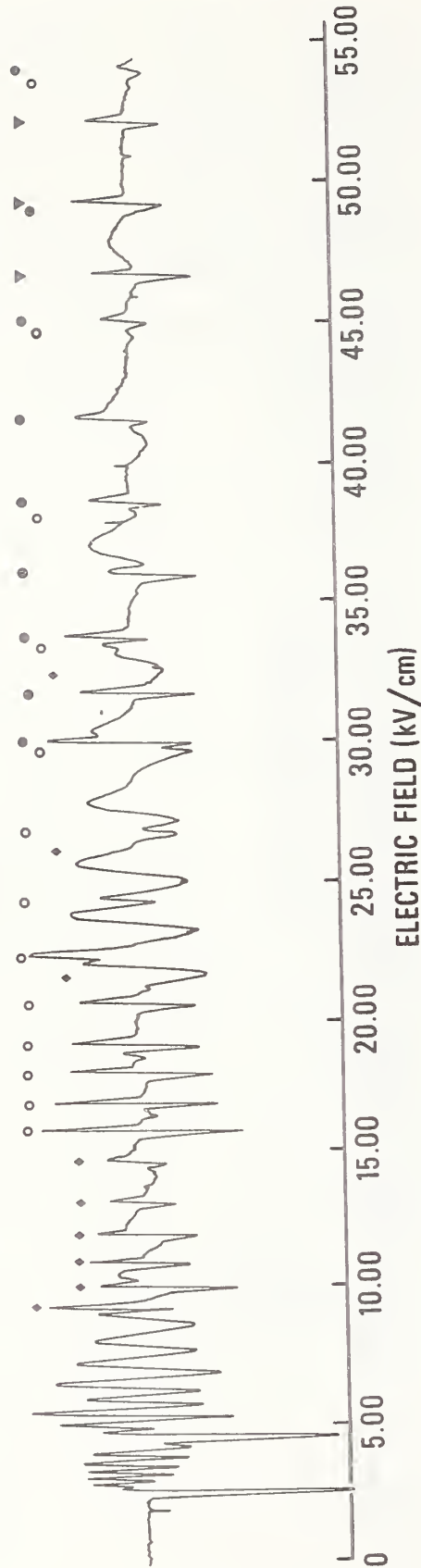


Figure A8. Stark spectrum of formaldehyde taken on the R(14), 9.6 μm , CO_2 laser line. The symbols identify M_J components of the following lines: ♦:J=14; ○:J=17; ●:J=18; ▼:J=19. The J=15 and 16 lines are crowded below 10 kV/cm.

OFFICIAL USE ONLY

The detector was a commercially available (Hg,Cd) Te photoconductive detector with a matched preamplifier and a D_{λ}^* of approximately 2×10^{10} cm Hz^{1/2}/watt.

Results

High resolution spectra were obtained in two polarizations. For one series the laser light was polarized perpendicular to the Stark field and covered laser lines P(34), P(12), P(10), P(8), and R(10)-R(16) in the 9.6 μ m band. For the other series the Stark plates were rotated so that the light was parallel to the Stark field. This latter series included the P(34), P(32), P(12), R(10)-R(16), and R(20)-R(32) laser lines in the 9.6 μ m band. Several of the spectra as taken directly from the charts are shown in figures A7 and A8. Close examination of these charts reveals the detail and resolution of this technique, as well as the sensitivity. The signal to noise ratio for high J ($J > 20$) transitions is quite good, since for high J transitions the ground state thermal population is small and this population must be further partitioned among the $(2J+1)$ sublevels.

Data were derived from the charts, tabulated, and line identification, for most of the assigned lines, was done graphically. For $\Delta M = 0$ transitions $1/E$ for successive

OFFICIAL USE ONLY

components was plotted vs. successive integers, M_J , to obtain a straight line. The value of M_{\max} , and thus the entire axis, was adjusted so that the line passed through (0,0) [see eqs. (14-16)]. One such plot is shown in figure A9, and in general illustrates the elegances and precision of this technique. The plot of $1/E$ vs. M is a straight line regardless of whether $\Delta M=0$ or ± 1 , so the measured values of $1/E$ were fit via a linear regression analysis to a linear function of M . These results are presented in table A1. If the Stark effect is strictly first order some information, such as Δv and $(\tilde{B}' - \tilde{B}'')$, can be obtained from these data. A measure of adequacy of the assumption of first order can be gotten by the value of intercept/slope for $\Delta M = \pm 1$ lines. For example, for all $P_{Q_5}(J)$ lines, the magnitude of the ratio intercept/slope should equal 4, which it does for $P_{Q_5}(5) - P_{Q_5}(8)$. However, note that for the higher J values this does not hold, which indicates a departure from the first order approximation for higher J states.

To the extent that the first order Stark effect is valid (e.g., for low J) one can calculate Δv from eq. (15). From this one can obtain the frequency of the line by using the relation $\nu_J = \nu_L - \Delta v$ if one knows the sign of Δv by other means. This information can be obtained by performing a "pulling" experiment, i.e., the laser is taken out of feedback control

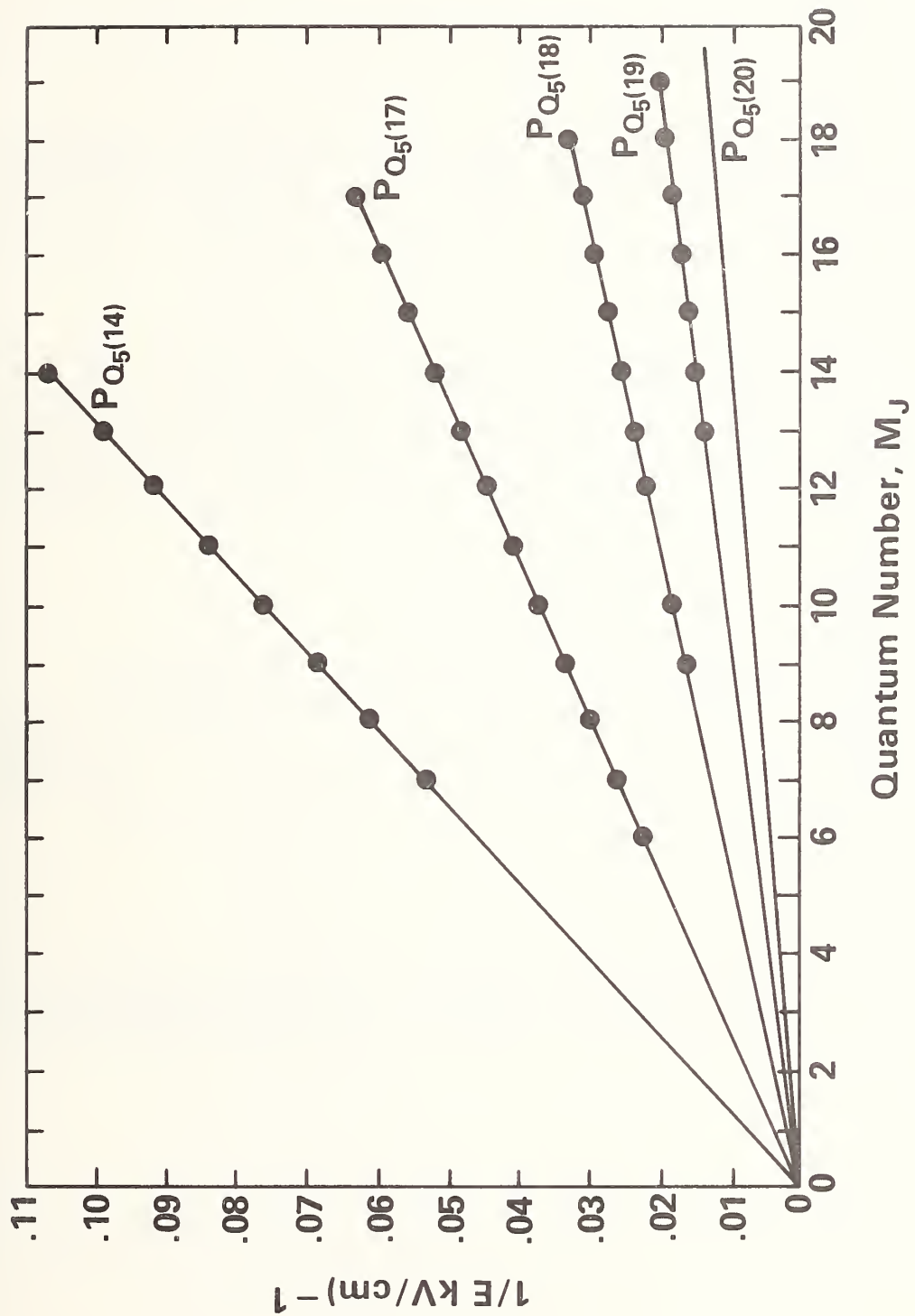


Figure A9. Plot $1/E$ vs. M_J for the spectrum in figure A8.

Table A1. Linear regression analysis for formaldehyde.

Laser Line	Polarization	Probable Line Assignment	Intercept (kv/cm) ⁻¹	Slope (kv/cm) ⁻¹	Standard deviation (S _{y,x})	M _{Jmax}
P (34)	A	P _{P5} (17)	-1.558 x 10 ⁻³	4.590 x 10 ⁻³	3.6 x 10 ⁻⁵	--
P (34)	A	P _{P5} (17)	2.61 x 10 ⁻³	4.494 x 10 ⁻³	4.6 x 10 ⁻⁴	--
P (34)	A	P _{P5} (17)	1.78 x 10 ⁻³	4.583 x 10 ⁻³	4.1 x 10 ⁻⁵	--
P (34)	B	P _{P5} (17)	-6 x 10 ⁻⁶	4.592 x 10 ⁻³	4.4 x 10 ⁻⁵	--
P (32)	B	P _{P5} (16)	-1.3 x 10 ⁻⁴	4.273 x 10 ⁻³	6.4 x 10 ⁻⁵	15
P (12)	B	P _{P4} (18)	4 x 10 ⁻⁵	4.498 x 10 ⁻³	5.6 x 10 ⁻⁵	17
P (12)	A	P _{P4} (18)	5 x 10 ⁻⁴	4.550 x 10 ⁻³	1 x 10 ⁻⁴	18
R (10)	B	--	--	4.198 x 10 ⁻³	1.3 x 10 ⁻⁴	22
R (12)	B	--	1.6 x 10 ⁻³	5.450 x 10 ⁻³	9.5 x 10 ⁻⁵	19
R (12)	B	P _{P3} (18)	1.3 x 10 ⁻⁴	1.613 x 10 ⁻³	7.5 x 10 ⁻⁵	18
R (12)	A	--	6.0 x 10 ⁻³	5.522 x 10 ⁻³	1 x 10 ⁻⁴	18
R (12)	A	--	-3.8 x 10 ⁻³	5.438 x 10 ⁻³	5.7 x 10 ⁻⁴	19
R (14)	B	P _{Q5} (14)	2.6 x 10 ⁻³	7.597 x 10 ⁻³	8.7 x 10 ⁻⁵	14
R (14)	B	P _{Q5} (17)	2 x 10 ⁻⁵	3.728 x 10 ⁻³	6.9 x 10 ⁻⁵	17
R (14)	B	P _{Q5} (18)	3 x 10 ⁻⁵	1.849 x 10 ⁻³	3.0 x 10 ⁻⁵	18
R (14)	B	P _{Q5} (19)	-9 x 10 ⁻⁶	1.126 x 10 ⁻³	3.9 x 10 ⁻⁶	19
R (14)	B	P _{Q5} (20)	-2 x 10 ⁻⁵	7.528 x 10 ⁻⁴	--	20
R (14)	A	P _{Q5} (15)	-9.5 x 10 ⁻³	14.01 x 10 ⁻³	5.7 x 10 ⁻⁴	14
R (14)	A	P _{Q5} (16)	--	22.50 x 10 ⁻³	8.4 x 10 ⁻⁴	15
R (16)	A	P _{Q5} (5)	.05827	.01484	1.1 x 10 ⁻⁴	5

Table A1 (con't)

Laser Line	Polarization	Probable Line Assignment	Intercept (kV/cm) ⁻¹	Slope (kV/cm) ⁻¹	Standard deviation (S.V.%)	M _{Jmax}
R(16)	A	P _Q ₅ (6)	.02554	6.496 x 10 ⁻³	1.4 x 10 ⁻⁴	6
R(16)	A	P _Q ₅ (7)	.01317	3.283 x 10 ⁻³	8.4 x 10 ⁻⁶	7
R(16)	A	P _Q ₅ (8)	7.51 x 10 ⁻³	1.857 x 10 ⁻³	7.2 x 10 ⁻⁶	8
R(16)	B	P _Q ₅ (5)	2 x 10 ⁻³	.01494	3.7 x 10 ⁻⁴	5
R(16)	B	P _Q ₅ (6)	8 x 10 ⁻⁵	6.521 x 10 ⁻³	1.6 x 10 ⁻⁴	6
R(16)	B	P _Q ₅ (7)	3 x 10 ⁻⁵	3.336 x 10 ⁻³	9.6 x 10 ⁻⁵	7
R(16)	B	P _Q ₅ (8)	--	1.882 x 10 ⁻³	--	8
R(20)	B	P _P ₃ (26)	1.5 x 10 ⁻⁵	9.118 x 10 ⁻⁴	1.3 x 10 ⁻⁵	26
R(20)	B	P _P ₃ (24)	-7.6 x 10 ⁻⁵	8.746 x 10 ⁻⁴	8.6 x 10 ⁻⁶	24
R(22)	B	P _P ₃ (21)	-9 x 10 ⁻⁶	2.466 x 10 ⁻³	6.8 x 10 ⁻⁵	21
R(22)	B	P _P ₃ (22)	-3 x 10 ⁻⁵	2.176 x 10 ⁻³	3.4 x 10 ⁻⁵	22
R(22)	B	P _P ₃ (20)	-7 x 10 ⁻⁵	9.271 x 10 ⁻⁴	1.9 x 10 ⁻⁶	20
R(22)	B	P _P ₃ (23)	6.5 x 10 ⁻⁵	6.6 x 10 ⁻⁴	--	23
R(24)	B	P _P ₃ (17)	-5 x 10 ⁻⁴	6.938 x 10 ⁻³	7.5 x 10 ⁻⁵	17
R(24)	B	P _P ₃ (18)	-3 x 10 ⁻⁴	3.714 x 10 ⁻³	9.4 x 10 ⁻⁵	18
R(24)	B	P _P ₃ (16)	-9 x 10 ⁻⁵	2.309 x 10 ⁻³	1.2 x 10 ⁻⁵	16
R(24)	B	P _P ₃ (15)	2 x 10 ⁻⁶	1.636 x 10 ⁻³	1.6 x 10 ⁻⁵	15
R(24)	B	P _P ₃ (19)	5 x 10 ⁻⁵	1.181 x 10 ⁻³	1.8 x 10 ⁻⁵	19
R(24)	B	P _P ₃ (14)	2 x 10 ⁻⁷	1.427 x 10 ⁻³	4 x 10 ⁻⁶	14
R(26)	B	--	-2 x 10 ⁻³	.0562	3.1 x 10 ⁻³	9
R(26)	B	--	-5 x 10 ⁻⁴	.01687	1.4 x 10 ⁻⁴	10
R(26)	B	--	3.7 x 10 ⁻⁴	7.822 x 10 ⁻³	3.4 x 10 ⁻⁵	11
R(26)	B	--	2 x 10 ⁻⁴	4.309 x 10 ⁻³	6 x 10 ⁻⁵	12
R(26)	B	--	-3 x 10 ⁻⁵	2.620 x 10 ⁻³	2 x 10 ⁻⁵	13

Table A1 (con't)

Laser Line	Polarization	Probable Line Assignment	Intercept (kV/cm) ⁻¹	Slope (kV/cm) ⁻¹	Standard deviation (S·X)	M _{Jmax}
R(26)	B	--	-1 x 10 ⁻⁴	1.687 x 10 ⁻³	1.8 x 10 ⁻⁵	14
R(28)	B	--	-7 x 10 ⁻⁴	.0154	2.8 x 10 ⁻⁴	11
R(28)	B	--	-8 x 10 ⁻⁵	7.149 x 10 ⁻³	7.6 x 10 ⁻⁵	10
R(28)	B	--	-5 x 10 ⁻⁵	2.191 x 10 ⁻³	3.8 x 10 ⁻⁶	12
R(28)	B	--	5 x 10 ⁻⁵	1.236 x 10 ⁻³	6.9 x 10 ⁻⁶	16
R(30)	B	--	4 x 10 ⁻⁴	^a .0191	3 x 10 ⁻⁴	13
R(30)	B	--	1 x 10 ⁻⁴	2.128 x 10 ⁻³	2.8 x 10 ⁻⁶	12
R(30)	B	--	-8 x 10 ⁻⁶	1.483 x 10 ⁻³	3.2 x 10 ⁻⁶	14
R(32)	B	--	-1 x 10 ⁻⁶	3.153 x 10 ⁻³	2 x 10 ⁻⁵	15
R(32)	B	--	3 x 10 ⁻⁴	2.079 x 10 ⁻³	6.4 x 10 ⁻⁶	16
R(32)	B	--	7 x 10 ⁻⁵	1.813 x 10 ⁻³	5 x 10 ⁻⁵	14

*A: Perpendicular polarization
 B: Parallel polarization

Note: -- indicates incomplete data.

OFFICIAL USE ONLY

and the PZT bias is adjusted so that the laser is operating on one side of the gain profile. Under these conditions (for short periods of time) the frequency is shifted a small amount in a direction that is known from the physical characteristics of the PZT. In this case a larger bias voltage on the PZT lengthens the cavity and reduces the frequency. A laser Stark spectrum is then taken, compared to the original and the sign of $\Delta\nu$ deduced. Such an experiment was done for $P_{Q_5}(5)$ on R(16). When the cavity was lengthened the pattern shifted toward zero field, indicating that $\nu_J < \nu_L$.

Referring to eq. (5), for a P_Q branch, the energies in the symmetric top approximation, ignoring terms in D_J , D_{JK} and D_K , are given by

$$E_4^{\circ}(J,K) - E_0^{\circ}(J,K-1) = \nu_4 + (\Delta A - \Delta \bar{B})K^2 - (A' - \bar{B}') (2K-1) + \Delta \bar{B}J(J+1)$$

where $\Delta A = A' - A''$ and $\Delta \bar{B} = B' - B''$. Then, for energy differences between lines in the same branch,

$$E(J_1'', K'') - E(J_2'', K'') = \Delta \bar{B} \left[J_1''(J_1''+1) - J_2''(J_2''+1) \right] = \delta$$

or, letting $J_2'' = J_1'' + \Delta J$,

$$\delta = -\Delta \bar{B} \Delta J (2J_1'' + J_1'' + 1)$$

OFFICIAL USE ONLY

$P_{Q_5}(5) - P_{Q_5}(8)$ were used to calculate $\Delta\bar{B}$, and the results are given below:

$$\begin{array}{ll}
 P_{Q_5}(5) - P_{Q_5}(6) = +.05590 & \Delta\bar{B} = -.004658 \\
 P_{Q_5}(6) - P_{Q_5}(7) = +.06897 & \Delta\bar{B} = -.004926 \\
 P_{Q_5}(7) - P_{Q_5}(8) = +.07990 & \Delta\bar{B} = -.004994 \\
 P_{Q_5}(5) - P_{Q_5}(7) = +.12491 & \Delta\bar{B} = -.004804 \\
 P_{Q_5}(5) - P_{Q_5}(8) = +.20481 & \Delta\bar{B} = -.004876
 \end{array}
 \left. \vphantom{\begin{array}{l} \\ \\ \\ \\ \end{array}} \right\} \text{(Avg. } -.004859)$$

The average value of $\Delta\bar{B}$ (-0.004859) is to be compared with the value of $-0.005810 \text{ cm}^{-1}$ as calculated from the reported constants [5,9]. This significant difference probably reflects the shortcomings of the approximations used.

One can also use the value of $\Delta\nu$ to obtain the transition frequency with a reasonably high accuracy for the low J transitions and from this calculate the Coriolis coupling constant, $\xi_{6,4}^\alpha$. Using this symmetric top approximation the value of $\xi_{6,4}^0$ in eq. (6) can be calculated more precisely than either E_6^0 or E_4^0 . From eqs. (8) and (9), then $\xi_{6,4}^\alpha$ is found to be 10.405 cm^{-1} . This is in agreement with a value of $\xi_{6,4}^\alpha = 10.340 \pm 0.082$ calculated by Nakagawa and Morino [9].

While little new information has been obtained from the limited spectra obtained to date, this technique has been shown to be adequate for line identification and has the potential

OFFICIAL USE ONLY

for accurate spectral information. Since little is known about the isotope shift of C-13 substituted formaldehyde (or other small molecules of this type) the ability to make line identifications and derive spectral information by using this technique is important. Furthermore, the techniques learned by doing formaldehyde are applicable to other near-symmetric rotors which include a variety of molecules of interest, such as methyl mercaptan, for which no high resolution data are available in the literature.

OFFICIAL USE ONLY

References--Appendix A

1. H. H. Blau and J. H. Nielsen, *J. Mol. Spectrosc.* 1, 124 (1957).
2. T. Oka, K. Takagi and Y. Morino, *J. Mol. Spectrosc.* 14, 27 (1964).
3. T. Nakagawa, H. Kashiwagi, H. Kurihara, and Y. Morino, *J. Mol. Spectrosc.* 31, 436 (1969).
4. K. Yamada, T. Nakagawa, K. Kuchitsu, and Y. Morino, *J. Mol. Spectrosc.* 38, 70 (1971).
5. D. R. Johnson, F. J. Lovas and W. H. Kirchhoff, *J. Phys. Chem. Ref. Data*, 1, 1011 (1972).
6. J. W. C. Johns and A. R. W. McKellar, *J. Mol. Spectrosc.* 48, 354 (1973).
7. J. W. C. Johns and A. R. W. McKellar, *J. Chem. Phys.* 63, 1682 (1975).
8. W. L. Smith and I. M. Mills, *J. Mol. Spectrosc.* 11, 11 (1963).
9. T. Nakagawa and Y. Morino, *J. Mol. Spectrosc.* 38, 84 (1971).
10. For a discussion of the spectroscopy of asymmetric and near symmetric rotors see Townes and Schalow, Microwave Spectroscopy, McGraw-Hill (N.Y.) 1965.
11. N. L. Alpert, W. E. Keiser and H. A. Szymanski, IR Theory and Practice of Infrared Spectroscopy, Plenum Press (NY) 1970.

U.S. DEPT. OF COMM. BIBLIOGRAPHIC DATA SHEET	1. PUBLICATION OR REPORT NO. NBS IR 78-1510	2. Gov't. Accession No.	3. Recipient's Accession No.
4. TITLE AND SUBTITLE Intruder Detection Using Trace Constituent Analysis		5. Publication Date May 1979	
7. AUTHOR(S) J. R. DeVoe, D. M. Sweger, R. A. Velapoldi		6. Performing Organization Code	
9. PERFORMING ORGANIZATION NAME AND ADDRESS NATIONAL BUREAU OF STANDARDS DEPARTMENT OF COMMERCE WASHINGTON, DC 20234		8. Performing Organ. Report No.	
12. SPONSORING ORGANIZATION NAME AND COMPLETE ADDRESS (Street, City, State, ZIP) Nuclear Surety Directorate Defense Nuclear Agency Washington, D.C. 20305		10. Project/Task/Work Unit No.	
15. SUPPLEMENTARY NOTES <input type="checkbox"/> Document describes a computer program; SF-185, FIPS Software Summary, is attached.		11. Contract/Grant No.	
16. ABSTRACT (A 200-word or less factual summary of most significant information. If document includes a significant bibliography or literature survey, mention it here.) This report documents the progress made during the first year (fiscal year 1977) of a project to develop intruder tagging and taggant detection systems for use as a component of the Forced Entry Deterrent Systems (FEDS) being developed by the Defense Nuclear Agency to protect nuclear weapons in storage. Several tagging and detection techniques were investigated. Glass microsphere particle tags doped with rare earths were fabricated, and a microspectrofluorimeter was used to characterize the luminescence spectra and determine the detection sensitivity limits for these uniquely coded particles. Dispensing systems and prototype field detection instrumentation for particle tagging were also considered. Initial experiments to develop a gaseous tagging system were directed toward establishing the limits of detection and the feasibility of isotopic ratio measurements by the absorption of infrared radiation. The results obtained in the measurement of the $^{12}\text{C}/^{13}\text{C}$ ratio using a Stark-modulated CO_2 gas laser system and a semiconductor diode laser system are described, and the theoretical development of techniques for spectral line assignment for simple molecules is discussed in detail. Concepts for the real-time remote monitoring of trace constituents in the environment surrounding a storage facility and the detection of contaminating gases are presented. Preliminary research directed toward the ultimate development of an olfactory sensor transducer is briefly discussed.		13. Type of Report & Period Covered	
17. KEY WORDS (six to twelve entries; alphabetical order; capitalize only the first letter of the first key word unless a proper name; separated by semicolons) Fluorescence; infrared absorption spectra; isotopic ratio measurement; laser infrared absorption; luminescence; olfactory sensing; tagging; trace constituent analysis; vibration-rotation energy levels.		14. Sponsoring Agency Code	
18. AVAILABILITY <input type="checkbox"/> Unlimited <input checked="" type="checkbox"/> For Official Distribution. Do Not Release to NTIS <input type="checkbox"/> Order From Sup. of Doc., U.S. Government Printing Office, Washington, DC 20402, SD Stock No. SN003-003- <input type="checkbox"/> Order From National Technical Information Service (NTIS), Springfield, VA. 22161	19. SECURITY CLASS (THIS REPORT) UNCLASSIFIED	21. NO. OF PRINTED PAGES	
20. SECURITY CLASS (THIS PAGE) UNCLASSIFIED	22. Price		





